Aberrant cortical activity, functional connectivity, and neural assembly architecture after photothrombotic stroke in mice

Mischa V. Bandet,[1,2,3] and Ian R. Winship[1,2,3*]

[1]Neuroscience and Mental Health Institute
[2]Neurochemical Research Unit
[3]Department of Psychiatry
University of Alberta, Edmonton, Alberta T6G 2B7, Canada

Keywords: stroke**;** photothrombosis; two-photon; calcium imaging; gcamp; somatosensory cortex; neural assemblies; ensembles; limb-associated

Running Title: Aberrant cortical activity, functional connectivity, and neural assembly architecture after stroke

***Corresponding Author:**
Dr. Ian R. Winship
Professor
Department of Psychiatry
12-127 Clinical Sciences Building
University of Alberta
Edmonton, AB
Canada, T6G 2G3
Phone: 780-492-8658
Fax: 780-492-6841
iwinship@ualberta.ca

Abstract

Despite substantial progress in mapping the trajectory of network plasticity resulting from focal ischemic stroke, the extent and nature of changes in neuronal excitability and activity within the peri-infarct cortex of mice remains poorly defined. Most of the available data have been acquired from anesthetized animals, acute tissue slices, or infer changes in excitability from immunoassays on extracted tissue, and thus may not reflect cortical activity dynamics in the intact cortex of an awake animal. Here, *in vivo* two-photon calcium imaging in awake, behaving mice was used to longitudinally track cortical activity, network functional connectivity, and neural assembly architecture for 2 months following photothrombotic stroke targeting the forelimb somatosensory cortex. Sensorimotor recovery was tracked over the weeks following stroke, allowing us to relate network changes to behavior. Our data revealed spatially restricted but long-lasting alterations in somatosensory neural network function and connectivity. Specifically, we demonstrate significant and long-lasting disruptions in neural assembly architecture concurrent with a deficit in functional connectivity between individual neurons. Reductions in neuronal spiking in peri-infarct cortex were transient but predictive of impairment in skilled locomotion measured in the tapered beam task. Notably, altered neural networks were highly localized, with assembly architecture and neural connectivity relatively unaltered a short distance from the peri-infarct cortex, even in regions within ‘remapped’ forelimb functional representations identified using mesoscale imaging with anaesthetized preparations 8-weeks after stroke. Thus, using longitudinal two photon microscopy in awake animals, these data show a complex spatiotemporal relationship between peri-infarct neuronal network function and behavioural recovery. Moreover, the data highlight an apparent disconnect between dramatic functional remapping identified using strong sensory stimulation in anaesthetized mice compared

to more subtle and spatially restricted changes in individual neuron and local network function in awake mice during stroke recovery.

Introduction

Investigations of the excitability of neurons in the peri-infarct cortex during recovery from ischemic stroke have yielded a complex and at times contradictory data set. Peri-infarct hyper-excitability was suggested by data from anesthetized rats that exhibited elevated spontaneous multiunit firing within peri-infarct regions 3-7 days after stroke [1]. Similarly, downregulated GABAergic inhibition in peri-infarct cortex [1–6], degeneration of parvalbumin-positive inhibitory interneurons [3,7], decreased paired pulse inhibition [8–10], increased NMDA receptor mediated excitation [11,12], and a downregulation of KCC2 [13–17] have suggested that the peri-infarct cortex is hyper-excitable during recovery, contributing to increased risk of epileptogenesis in the post stroke brain [13,18]. Conversely, several groups have reported that the sensory-evoked responsiveness of the peri-infarct cortex is diminished during recovery from focal photothombotic stroke [19–25]. Even after months of recovery following forelimb (FL) representation targeted stroke, the remapped representation of the FL has been shown to display prolonged modes of activation with lower amplitude [19] and reduced temporal fidelity [23].

Almost all studies that have examined post-stroke cortical responsiveness have used surgical preparations with anesthetized animals. Anesthesia disrupts cortical activity dynamics and functional connectivity between cortical areas [26–30], and has been shown to reduce the magnitude and spread of cortical activation from sensory stimuli [31–39]. It further reduces the potential contribution of corollary discharge and reafference due to voluntary action in modulating sensory input and cortical responses [40]. It has also recently been shown that the propagation pattern of cortical activity differs between evoked and spontaneous activity, with spontaneous activity showing more complex trajectories and lower activity amplitudes [41].

Somatosensory responses are known to be modulated by the relevance of stimuli to behavior and task performance [42–47], and by corollary feedback during [48], or even before [49–51], the onset of movement. Together, these studies point to a complex, interconnected system that modulates the activity of somatosensory networks in the awake behaving animal that is either not present, or is altered, in studies of evoked cortical activity under the anesthetized state. While monitoring cortical activity in awake mobile animals presents methodological complexity, it avoids confounds associated with the anesthetized state and provides unique insight into evolving patterns of network activity that may be unique to the awake state.

To investigate neural activity patterns during stroke recovery while avoiding the potential confounds of anesthesia, the present work used two photon Ca^{2+} imaging within and distal to the peri-infarct region of a focal photothrombotic stroke lesioning the FL primary somatosensory cortex in mice. We used awake, behaving but head-fixed mice in a mobile homecage to longitudinally measure cortical activity, then used computational methods to assess functional connectivity and neural assembly architecture at baseline and each week for 2 months following stroke. Behavioral recovery from stroke was measured in the same animals on a tapered beam task and string pull task to determine the time course of sensorimotor deficits related to changes in cortical activity and network architecture. Our goal was to use longitudinal imaging and advanced computational analyses to define network changes in somatosensory cortex associated with sensorimotor recovery. We show that despite disturbances to the widefield topology and amplitude of the sensory-evoked FL map (acquired under anesthetic), it is only within the immediate peri-infarct region after FL targeted stroke that neural activity, functional connectivity, and neural assembly architecture are disrupted. We demonstrate that the peri-infarct

somatosensory cortex displays a marked reduction in neural assembly number, an increase in neural assembly membership, and persistent alterations in assembly-assembly correlations, and that this occurs alongside transient deficits in both functional connectivity and neural activity. Notably, we show that reduced neuronal spiking is strongly correlated with a deficit in motor performance on the tapered beam task. Surprisingly, we also show that significant alterations in neuronal activity (firing rate), functional connectivity, and neural assembly architecture are absent within more distal regions of cortex as little as 750 µm from the stroke border, even in areas identified by regional functional imaging (under anaesthesia) as 'remapped' locations of sensory-evoked FL activity 8-weeks post-stroke.

Results

The experimental timeline is illustrated in Fig 1A. Adult Thy1-GCaMP6S mice were implanted with chronic cranial windows and habituated on the floating homecage, tapered beam and string pull task (Fig 1A-C). The cFL and cHL somatosensory areas were mapped on the cortex using widefield Ca^{2+} imaging of sensory-evoked activity in isoflurane anaesthetized mice (Fig 1D, 2A, see methods). Regions of interest for longitudinal awake two-photon Ca^{2+} imaging of cellular activity (Fig 1E) were chosen based on these pre-stroke widefield Ca^{2+} limb maps (Fig 2). The first imaging region of interest was located at the boundary of the pre-stroke cFL and cHL somatosensory maps (termed "peri-infarct" region based on its proximal location to the photothrombotic infarct after stroke) and the second region as lateral to the pre-stroke cHL map (termed "distal" region due to its distance from the stroke boundary). These regions were imaged at baseline, and each week following photothrombotic stroke. Notably, these regions of interest incorporated the predicted areas of remapping for the limb associated somatosensory

representations after focal cFL cortex stroke based on previous studies [25,52]. Photothrombosis was directed to the cFL somatosensory representation as identified by regional imaging. Resulting infarcts lesioned this region, and borders were delineated by a region of decreased light absorption 1-week post-stroke (Fig 1D, Top). Within the peri-infarct imaging region, cellular dysmorphia and swelling was visually apparent in some cells during two photon imaging 1-week after stroke, but recovered over the 2 month post-stroke imaging timeframe (data not shown). These gross morphological changes were not visually apparent in the more distal imaging region lateral to the cHL.

Altered sensory-evoked widefield Ca^{2+} maps after stroke

Regional remapping of the limb-associated somatosensory cortex occurs over the weeks following focal cortical stroke [25,52]. Here, widefield Ca^{2+} imaging of the cranial window in isoflurane anaesthetized mice was performed during piezoelectric stimulation of the contralateral limbs prior to stroke (to define the region targeted for infarction as described above), and at the 8-week post-stroke timepoint (to define regional remapping of the forelimb representation; see Fig 2A and Methods). Fig 2A shows representative montages from a stroke animal illustrating the cortical cFL and cHL Ca^{2+} responses to 1s, 100Hz limb stimulation of the contralateral limbs at the pre-stroke and 8-week post-stroke timepoints. The location and magnitude of the cortical responses changes drastically between timepoints, with substantial loss of supra-threshold activity within the pre-stroke cFL representation located anterior to the cHL map, and an apparent shift of the remapped representation into regions lateral to the cHL representation at 8-weeks post-stroke. A significant decrease in the cFL evoked Ca^{2+} response amplitude was observed in the stroke group at 8-weeks post-stroke relative to pre-stroke (Fig 2B). This is in

agreement with past studies [19–25], and suggests that cFL targeted stroke reduces forelimb evoked activity across the cFL somatosensory cortex in anaesthetized animals even after 2 months of recovery. There was no statistical change in the average size of cFL evoked representation 8-weeks after stroke (Fig 2C), but a significant posterior shift of the supra-threshold cFL map was detected (Fig 2D). Unmasking of previously sub-threshold cFL responsive cortex in areas posterior to the original cFL map at 8-weeks post-stroke could contribute to this apparent remapping. However, the amplitude of the cFL evoked widefield Ca^{2+} response in this distal region at 8-weeks post-stroke remains reduced relative to pre-stroke activation (Fig 2E). Previous studies suggest strong inhibition of cFL evoked activity during the first weeks after photothrombosis [25]. Without longitudinal measurement in this study to quantify this reduced activation prior to 8-weeks post-stroke, we cannot differentiate potential remapping due to unmasking of the cFL representation that enhances the cFL-evoked widefield Ca^{2+} response from apparent remapping that simply reflects changes in the signal-to-noise ratio used to define the functional representations. There were no group differences between stroke and sham groups in cHL evoked intensity, area, or map position (data not shown).

Impaired performance on tapered beam but not string pull after focal somatosensory stroke

Post-stroke sensorimotor impairment was measured on the tapered beam task and string pull task. In the tapered beam, errors (slips off the beam), indicative of post-stroke impairment, were tracked as the number of left (affected) side slips, right (non-affected) side slips, and the distance to first slip (Fig 3A). We observed a significant interaction of group and time in the number of left side (contralesional) slips (Fig 3B), with *post-hoc* comparisons confirming

increased left slips at 1-week post-stroke compared to baseline and compared to 1-week in sham. Consistent with the unilateral nature of the photothrombotic damage to the cortex in this study, no main effects or interaction was seen in the number of right side slips (Fig 3C). No main effects or interaction was observed in the distance to first slip (Fig 3D). These results are consistent with a transient deficit in motor behavior on the tapered beam during the first week after stroke induced by focal cortical lesion to the sensorimotor cortex [53,54], as opposed to more sustained deficits observed in models of middle cerebral artery occlusion [55,56]. In contrast to previous studies investigating string pull after stroke [57], we did not detect a significant effect of photothrombosis on any kinematic parameters during string pulling (Fig S1).

Firing rate of neurons in the peri-infarct cortex correlates with performance on the tapered beam task

The firing rate of cortical somatosensory neurons in our awake behaving animals (Fig 4A) was calculated using a custom Matlab algorithm to identify ‘significant’ calcium transients [58,59] and the mean firing rate of the sampled neural population during periods of movement and periods of rest in the mobile homecage. The average firing rate in the peri-infarct region during recovery in movement and rest is illustrated in Figures 4B and 4C, respectively. A significant main effect of group on firing rate was detected at rest (Fig 4C). *Post-hoc* comparisons confirmed significantly reduced average firing rate when moving and at rest at 1-week in the stroke group compared to pre-stroke (Fig 4B and 4C, respectively). Notably, firing rate at 1-week post-stroke during movement and at rest were significantly negatively correlated with the number of left slips in the tapered beam at the same 1-week timepoint (Fig 4D and 4E). No main effects or significant interaction was observed in the distal imaging region for either

movement or at rest (Fig 4F and 4G, respectively). Firing rate during movement and at rest at 1-week within the distal region was also not significantly correlated with left slips on the tapered beam at the same timepoint (Fig 4H and Fig 4I, respectively). These results indicate decreased neuronal spiking 1-week after stroke in regions immediately adjacent to the infarct, but not in distal regions, that is strongly related to sensorimotor impairment. This finding runs contrary to a previous report of increased spontaneous multi-unit activity as early as 3-7 days after focal photothrombotic stroke in the peri-infarct cortex [1], but is in agreement with recent single-cell calcium imaging data demonstrating reduced sensory-evoked activity in neurons within the peri-infarct cortex after stroke [60,61]. While the majority of neuronal activity occurred during movement, correlations between firing rate and animal movement were low and did not vary between stroke and sham groups (Fig S2).

Altered functional connectivity in the peri-infarct somatosensory cortex

Studies in humans and animals using mesoscale imaging methods indicate that stroke disrupts functional connectivity between widespread cortical regions [26,62–72]. However, few studies have examined functional connectivity at the level of local neural populations after focal stroke [73,74], and none have examined the primary somatosensory cortex. To define functional connectivity in local neural networks within the peri-infarct somatosensory cortex, we plotted the functional connectivity of the neural population in terms of the strength of their cell-cell correlations (Fig 5) and quantified the properties of these connections (Fig 6). We observed a significant loss of functional connectivity 1-week after stroke within the peri-infarct region. This was visually apparent in the stroke group functional connectivity plots at the 1-week timepoint (Fig 5A and 5B) compared to the same location in sham animals (Fig 5E and 5F). Notably, no

profound loss of functional connectivity is visually apparent in the distal region in the stroke (Fig 5C and 5D) or sham (Fig 5G and 5H) groups. Within the peri-infarct region, we observed a statistical trend of a main effect of time in the average number of 'significant' functional connections per neuron (Fig 6A; see Methods). *Post-hoc* comparisons confirmed a significantly reduced average number of significant connections per neuron at 1-week post-stroke compared to pre-stroke and to 1-week sham. We observed a significant main effect of time on the average number of strong connections (r>.3) per neuron (Fig 6B). *Post-hoc* comparisons confirmed strong connections were significantly reduced 1-week post-stroke relative to pre-stroke. In the distal region, no main effects or interaction was identified in the average number of significant connections per neuron (Fig 6D), highlighting regionally specific connectivity changes in individual neurons after stroke. However, we observed a significant main effect of time on the average number of strong (r>.3) connections per neuron in the distal region (Fig 6E), with *post-hoc* comparisons confirming that strong connections were significantly reduced 8-weeks post-stroke relative to pre-stroke. The deficit in significant connections between neurons for the peri-infarct region is consistent with a persistent deficit in functional connectivity lasting up to 30 days that was identified within the primary and supplementary motor cortex of mice using *in vivo* imaging after focal motor cortex stroke [73,74]. However, network density, defined as the ratio of measured significant functional network connections to the number of total possible network connections if all neurons were interconnected, was not decreased in either peri-infarct or distal regions in our study (Fig 6C and 6F, respectively). This is in contrast with previous research in the primary and supplementary motor cortex after focal motor cortex stroke that has demonstrated deficits in network density lasting up to 3-weeks post-stroke [74].

Neural assembly structure is disrupted in the peri-infarct region after stroke

The neural assembly hypothesis defines coordinated activity in groups of neurons as the basis for the representation of external and internal stimuli within the brain [75–77]. Likewise, perturbations within the structure and function of assemblies may signify aberrant processing of stimuli within neural networks, and is believed to play a significant role in the dysfunction observed in brain damage and neuropsychiatric diseases [76]. Although the use of sophisticated methods for detecting neural assemblies in large populations of neurons has gained increasing popularity with the advent of large population recordings using Ca^{2+} imaging [78], no previous studies have determined the longitudinal effects of stroke on the architecture of neural assemblies in cortex. To determine if focal stroke to the cFL cortex affects the properties of neural assemblies, we used a PCA-Promax procedure [58,59,78] for neural assembly detection to determine assembly size, population membership, assembly quantity, and overlap in assembly membership. The PCA-Promax method for determining neural assemblies allows neurons to participate in more than a single assembly [58,59], a property necessary to examine the ability of neural assemblies to dynamically form with varying members of the population for only brief periods of time [58,59,78]. Fig 7 shows representative neuronal Ca^{2+} fluorescence images with neural assemblies color coded and overlaid for each timepoint for the peri-infarct imaging region and for the distal imaging region for an example stroke and sham animal (Fig 7A and 7B, respectively). We observed a significant main effect of group on the number of assemblies in the peri-infarct imaging region (Fig. 8A). *Post-hoc* comparisons confirmed significantly reduced number of assemblies 1- and 4-weeks after stroke relative to sham controls (Fig 8A). *Post-hoc* comparisons also indicated a significant increase in the average number of neurons per assembly

at 1- and 2-weeks post-stroke relative to pre-stroke (Fig 8B). We further observed a statistical trend of a main effect of group in the average percent of the population per assembly (Fig 8C), with *post-hoc* tests indicating a statistical trend for 1-week post-stroke compared with pre-stroke. These data suggest that after stroke, neurons in peri-infarct cortex are functionally grouped into fewer distinct assemblies, with more neurons per assembly and more of the local network in the same assembly. For the distal imaging region, no differences in neural assembly properties were observed within and between the stroke and sham groups (Fig 8D-E).

Correlation between neural assembly activations is increased after stroke

If differential activation of neural assemblies in the naïve brain relates to representation of different aspects of the external world [58,75,77,79], then changes in the relationship between the activation patterns of assemblies may predict disrupted processing of sensory information within neural networks and how these networks differentially represent external stimuli. An increase in assembly size and reduction in assembly number might reflect a mechanism to replace lost function and increase somatic sensitivity, but may come at the cost of reduced stimulus specificity/fidelity within the network. The activation magnitude of assemblies can be correlated between assemblies over the recording period (Fig 9A). A significant main effect of group was detected in the assembly-assembly correlation coefficient (Fig 9B) in the peri-infarct cortex, with *post-hoc* tests indicating an increase in the correlation at 1-week post-stroke relative to pre-stroke and relative to 1-week in sham animals. No main effects or interaction was observed for the assembly-assembly correlation coefficient in the distal region (Fig 9C), suggesting that changes to assembly-assembly correlation were confined to the peri-infarct cortex. This increased tendency for functionally connected assemblies to be co-active after stroke

may reduce the signal to noise ratio for stimulus representation within the network and may reduce stimulus specificity within peri-infarct cortex. While assembly activations were often correlated with movement or rest periods (Fig S3), and 60% of assemblies in both the peri-infarct and distal regions were significantly correlated with animal movement at all time points (S3C and S3E, respectively), stroke did not change the average correlation between assembly activation and animal movement in either the peri-infarct (S3B Fig) or distal region (S3D Fig).

Discussion

Here, we used longitudinal two photon calcium imaging of awake, head-fixed mice in a mobile homecage to examine how focal photothrombotic stroke to the forelimb sensorimotor cortex alters the activity and connectivity of neurons adjacent and distal to the infarct. Consistent with previous studies using intrinsic optical signal imaging, mesoscale imaging of regional calcium responses (reflecting bulk neuronal spiking in that region) showed that targeted stroke to the cFL somatosensory area disrupts the sensory-evoked forelimb representation in the infarcted region. Consistent with previous studies, this functional representation exhibited a posterior shift 8-weeks after injury, with activation in a region lateral to the cHL representation. Notably, sensory-evoked cFL representations exhibited reduced amplitudes of activity relative to pre-stroke activation measured in the cFL representation and in the region lateral the cHL representation. Longitudinal two-photon calcium imaging in awake animals was used to probe single neuron and local network changes adjacent the infarct and in a distal region that corresponded to the shifted region of cFL activation. This imaging revealed a decrease in firing rate at 1-week post-stroke in the peri-infarct region that was significantly negatively correlated with the number of errors made with the stroke-affected limbs on the tapered beam task. Peri-

infarct cortical networks also exhibited a reduction in the number of functional connections per neuron and a sustained disruption in neural assembly structure, including a reduction in the number of assemblies and an increased recruitment of neurons into functional assemblies. Elevated correlation between assemblies within the peri-infarct region peaked 1-week after stroke and was sustained throughout recovery. Surprisingly, distal networks, even in the region associated with the shifted cFL functional map in anaesthetized preparations, were largely undisturbed.

Cortical plasticity after stroke

Plasticity within and between cortical regions contributes to partial recovery of function and is proportional to both the extent of damage, as well as the form and quantity of rehabilitative therapy post-stroke [80,81]. A critical period of highest plasticity begins shortly after the onset of stroke, is greatest during the first few weeks, and progressively diminishes over the weeks to months after stroke [19,82–86]. Functional recovery after stroke is thought to depend largely on the adaptive plasticity of surviving neurons that reinforce existing connections and/or replace the function of lost networks [25,52,87–89]. This neuronal plasticity is believed to lead to topographical shifts in somatosensory functional maps to adjacent areas of the cortex. The driver for this process has largely been ascribed to a complex cascade of intra- and extra-cellular signaling that ultimately leads to plastic re-organization of the microarchitecture and function of surviving peri-infarct tissue [52,80,84,88,90–92]. Likewise, structural and functional remodeling has previously been found to be dependent on the distance from the stroke core, with closer tissue undergoing greater re-organization than more distant tissue (for review, see [52]).

Previous research examining the region at the border between the cFL and cHL somatosensory maps has shown this region to be a primary site for functional remapping after cFL directed photothrombotic stroke, resulting in a region of cFL and cHL map functional overlap [25]. Within this overlapping area, neurons have been shown to lose limb selectivity 1-month post-stroke [25]. This is followed by the acquisition of more selective responses 2-months post-stroke and is associated with reduced regional overlap between cFL and cHL functional maps [25]. Notably, this functional plasticity at the cellular level was assessed using strong vibrotactile stimulation of the limbs in anaesthetized animals. Our findings using longitudinal imaging in awake animals show an initial reduction in firing rate at 1-week post-stroke within the peri-infarct region that was predictive of functional impairment in the tapered beam task. This transient reduction may be associated with reduced or dysfunctional thalamic connectivity [93–95] and reduced transmission of signals from hypo-excitable thalamo-cortical projections [96]. Importantly, the strong negative correlation we observed between firing rate of the neural population within the peri-infarct cortex and the number of errors on the affected side, as well as the rapid recovery of firing rate and tapered beam performance, suggests that neuronal activity within the peri-infarct region contributes to the impairment and recovery. The common timescale of neuronal and functional recovery also coincides with angiogenesis and re-establishment of vascular support for peri-infarct tissue [83,97–100].

Consistent with previous research using mechanical limb stimulation under anaesthesia [25], we show that at the 8-week timepoint after cFL photothrombotic stroke the cFL representation is shifted posterior from its pre-stroke location into the area lateral to the cHL map. Notably, our distal region for awake imaging was directly within this 8-week post-stroke

cFL representation. Despite our prediction that this distal area would be a hotspot for plastic changes, there was no detectable alteration to the level of population correlation, functional connectivity, assembly architecture or assembly activations after stroke. Moreover, we found little change in the firing rate in either moving or resting states in this region. Contrary to our results, somatosensory-evoked activity assessed by two photon calcium imaging in anesthetized animals has demonstrated an increase in cFL responsive neurons within a region lateral to the cHL representation 1-2 months after focal cFL stroke [25]. Notably, this previous study measured sensory-evoked single cell activity using strong vibrotactile (1s 100Hz) limb stimulation under aneasthesia [25]. This frequency of limb stimulation has been shown to elicit near maximal neuronal responses within the limb-associated somatosensory cortex under anesthesia [101]. Thus, strong stimulation and anaesthesia may have unmasked non-physiological activity in neurons in the distal region that is not apparent during more naturalistic activation during awake locomotion or rest. Regional mapping defined using strong stimulation in anesthetized animals may therefore overestimate plasticity at the cellular level.

Our results suggest a limited spatial distance over which the peri-infarct somatosensory cortex displays significant network functional deficits during movement and rest. Our results are consistent with a spatial gradient of plasticity mediating factors that are generally enhanced with closer proximity to the infarct core [84,88,90,91]. However, our analysis outside peri-infarct cortex is limited to a single distal area caudal to the pre-stroke cFL representation. Although somatosensory maps in the present study were defined by a statistical criterion for delineating highly responsive cortical regions from those with weak responses, the distal area in this study may have been a site of activity that did not meet the statistical criterion for inclusion in the

baseline map. The lack of detectable changes in population correlations, functional connectivity, assembly architecture and assembly activations in the distal region may reflect minimal pressure for plastic change as networks in regions below the threshold for regional map inclusion prior to stroke may still be functional in the distal cortex. Thus, threshold-based assessment of remapping may further overestimate the neuroplasticity underlying functional reorganization suggested by anaesthetized preparations with strong stimulation. Future studies could examine distal areas medial and anterior to the cFL somatosensory area, such as the motor and pre-motor cortex, to further define the effect of FL targeted stroke on neuroplasticity within other functionally relevant regions. Moreover, the restriction of these network changes to peri-infarct cortex could also reflect the small penumbra associated with photothrombotic stroke, and future studies could make use of stroke models with larger penumbral regions, such as the middle cerebral artery occlusion model. Larger injuries induce more sustained sensorimotor impairment, and the relationship between neuronal firing, connectivity, and neuronal assemblies could be further probed relative to recovery or sustained impairment in these models. Recent research also indicates that stroke causes distinct patterns of disruption to the network topology of excitatory and inhibitory cells [73], and that stroke can disproportionately disrupt the function of high activity compared to low activity neurons in specific neuron sub-types [61]. Mouse models with genetically labelled neuronal sub-types (including different classes of inhibitory interneurons) could be used to track the function of those populations over time in awake animals. A potential limitation of our data is the undefined effect of age and sex on cortical dynamics in this cohort of mice (with ages ranging from 3-9 months) after stroke. Aging can impair neurovascular coupling [102–107] and reduce ischemic tolerance [108–111], and greater investigation of cortical activity changes after stroke in aged animals would more effectively model stroke in humans. Future

research could replicate this study with mice in middle-age and aged mice (e.g. 9 months and 18+ months of age), and with sufficient quantities of both sexes, to better examine age and sex effects on measures of cortical function.

Altered network connectivity after stroke

A highly distributed network of neural circuits forms the basis of information flow in the mammalian brain [112,113]. Many disease states are thought to result in disturbances in neural dynamics and connectivity of these networks due to a process of randomization that affects the network nodes and connections, leading to degraded functional performance of the networks [113,114]. Most studies looking at the functional connectivity of cortical networks after stroke have focused on connectivity between cortical regions and few have looked at functional connectivity within neural populations at the single neuron level within a region of cortex. Our finding of decreased number of functional connections per neuron in the peri-infarct somatosensory cortex are consistent with recent research that demonstrated a decrease in the total number of functional connections for both inhibitory cells [73] and excitatory cells [73,74] in the motor and premotor cortex approximately 1-week after focal sensorimotor stroke. Reductions in strong functional connections between neurons in our experiments peaked 1-week after stroke, with only partial recovery over the next 7-weeks. These changes were restricted to peri-infarct cortex and were not observed in distal regions. As the cumulative total number of functional connections within a neural network is dependent on the number of cells measured from the population, it is possible that a decrease in the number of connections at early timepoints in both studies may either reflect a loss of neurons and/or the functional silencing of neurons within the imaged areas. Contrary to the findings from Bechay et al. [74], connection

density (as % of max possible connections) did not decrease in either the peri-infarct somatosensory cortex or distal somatosensory cortex after stroke in our study. Thus, we observed a significant reduction in the number of strong functional connections between neurons, but not a reduction in the density of connections. It is notable that the peak deficit in peri-infarct functional connectivity in our study occurs simultaneously with reduced neuronal firing and sensorimotor impairment. Early disruption has been reported in anaesthetized animals, and our data in awake animals demonstrates that early network changes may be a key contributor to dysfunction, and a restoration of spiking in peri-infarct regions is related to recovery [19–25].

Altered network dynamics after stroke

According to the cell assembly hypothesis, transient synchronous activation of distributed groups of neurons organize into “neural assemblies” that underly the representation of both external and internal stimuli in the brain [75]. These assemblies have been demonstrated in the mammalian [115–124] and zebrafish [58,125–127] brain, and are often similar in presentation between spontaneous and sensory evoked activations [58,115,120,128,129]. Indeed, the similarity between spontaneous assemblies and sensory evoked assemblies tends to increase during development [115], potentially illustrating the “sculpting” of neural circuits towards commonly encountered sensory stimuli. To date, however, no study has examined changes to the architecture of neural assemblies on the level of single cells within neural networks of the somatosensory cortex in the post-stroke brain. Our data shows a transient decrease in the number of assemblies and an increase in the number of neurons per assembly for the peri-infarct cortex after stroke. If assemblies within peri-infarct somatosensory cortex contribute to differential processing of distinct elements of sensory experience, a loss in the number of assemblies may

contribute to a loss in sensory range, as is observed in human stroke patients [130–134]. Although there have been calculations on the typical size of cell assemblies in several regions of the brain as a percentage of the network population (for review, see [75]), whether there is an optimal number of assemblies or optimal membership size of a neural assembly for a particular neural population is currently unknown. It is possible that a decrease in the number of assemblies and an increase in the membership of neurons in remaining assemblies may signify inefficient or ineffective forms of sensory processing. Likewise, it has been shown that electrical stimulation of single somatosensory neurons is sufficient to bias animal behavior towards a desired behavioral response [135,136], thereby suggesting that a sparse neural code may be sufficient for sensation. It has also been argued that minimizing correlation within the neural population serves to reduce representational redundancy and improves representational efficiency [137,138], thereby suggesting that fewer assemblies, with each containing more members, may be an inefficient form of representational coding for sensory information. Furthermore, we observed a persistent increase in the correlation between the activations of assemblies in the peri-infarct cortex that peaks 1-week post-stroke. Co-activation of multiple assemblies simultaneously may decrease the signal-to-noise ratio of the representational information that each specific assembly holds. It may further reduce efficient information transfer within and between cortical networks, and may relate to prolonged modes of somatosensory activation [19] and reduced fidelity in response to sensory stimuli observed in mouse models of focal FL stroke [23].

In summary, this work demonstrates that the peri-infarct region near to the stroke core displays decreased neuronal activity 1-week after stroke that is predictive of poor performance on the tapered beam task. Moreover, local neuronal networks immediately adjacent the stroke

exhibited reductions in functional connectivity and sustained alterations in the structure of neuronal assemblies, suggesting that focal injury leads to long lasting alterations in functional properties in local neuronal networks. Interestingly, altered connectivity and neuronal assembly structure was not detected in more distal cortical regions despite these regions being located within regions of cortex that appear to undergo functional remapping measured by cortical activation in response to vibrotactile limb stimulation in anaesthetized animals. The persistence of these distal networks during recovery highlights the importance of awake imaging and naturalistic stimuli to fully define functional network changes during recovery from nervous system injury.

Materials and Methods

Animals

Three to nine month old Thy1-GCaMP6S mice (Strain GP4.3, Jax Labs), N=16 stroke (average age: 5.4 months; 13 male, 3 female), and 5 sham (average age: 6 months; 3 male, 2 female), were used in this study. Mice were group housed in standard laboratory cages in a temperature-controlled room (23°C), maintained on a 12 hr light/dark cycle, and given standard laboratory diet and water *ad libitum*. Cages were randomly assigned to stroke or sham groups such that stroke and sham mice did not co-habitate the same cages. Animal weight was monitored daily during the entirety of the experiment. All experiments were approved by the University of Alberta's Health Sciences Animal Care and Use Committee and adhered to the guidelines set by the Canadian Council for Animal Care. Animals were euthanized through decapitation under deep urethane anesthesia following the end of the final imaging session.

Chronic cranial window implantation

Mice were implanted with a chronic cranial window [139] 4-weeks prior to the first imaging time point (Fig 1B). A surgical plane of anesthesia was achieved with 1.5% isofluorane. Body temperature was measured using a rectal probe and maintained at 37±0.5^{o}C. Mice were administered 0.15 mL of saline subcutaneously to maintain hydration levels. Dexamethasone (2 ug/g) was given subcutaneously to prevent cortical swelling and hemorrhaging during the craniotomy procedure. The skull was exposed by midline scalp incision and the skin retracted. The skull was gently scraped with a scalpel to remove the periosteum. Grooves were scraped into the skull surface to improve adhesion of dental cement to the skull. A 4 x 4 mm region of the skull overlying the right hemisphere somatosensory region was thinned to 25-50% of original thickness using a high-speed dental drill (~1-5mm lateral, +2 to -2 mm posterior to bregma). A dental drill was used to progressively thin the overlying skull until the bone could be removed with forceps, leaving the dura intact. The exposed cortical surface was bathed in sterile saline solution. A 5mm diameter coverslip was held in place over the craniotomy and its edges attached to the skull using cyanoacrylate glue. A metal headplate was positioned and secured to the skull using dental cement. Animals were injected subcutaneously with buprenorphine (1.0 mg/kg), removed from the isofluorane, and allowed to recover in a temperature-controlled recovery cage. Mice were returned to their home cage once recovered and monitored daily for weight and post-surgical signs for the duration of the chronic experiment. Mice were allowed to recover for a period of 2-weeks after window implantation prior to beginning behavior and task habituation (Fig 1C). Animals were excluded at the 2-week post-implantation timepoint if their cranial window became cloudy or non-imageable.

Tapered beam task habituation, testing and analysis

Methods for tapered beam habituation and automated recording and analysis have been described previously [53], with minor modification as follows. Nesting material from the homecage was placed inside of a dark box at the narrow end of the beam to motivate animals to cross the beam. For the first three sessions, mice were placed at the wide end of the beam and allowed to freely explore the beam for a period of 2 minutes, after which the experimenter placed a sheet of paper behind the animal as it crossed the beam to block its return path to the wide end and motivate it to cross to the narrow end with dark box. Once the mouse had reached the dark box with bedding material at the narrow end, they were given 60 seconds within the dark box to associate crossing the beam with reaching the safety of the dark box. The dark box was transported to their respective cage for the animal to further associate reaching the dark box with a safe transition to their cage. On subsequent days, mice were continuously run through the tapered beam for a period of 2 mins each, with a return to their cage after each crossing. On each of the 3 days prior to the first Ca^{2+} imaging session, mice were tested with three crossings of the beam per day to determine baseline crossing performance. Left and right-side slips were captured automatically by Raspberry Pi computer attached to touch sensors on the tapered beam, and Python scripts run to determine number of slips for each side and distance to first slip. Performance on the 9 baseline trials were average to determine a singular average baseline performance level. Mice were tested with three trials on each day prior to each weekly post-imaging timepoint to measure changes in performance.

String pull task habituation, testing and analysis

Methods for string pull habituation and testing have previously been described [140,141],

with modification as follows. For habituation, mice were individually placed in a transparent rectangular cage without bedding and allowed to freely explore for a period of 5 minutes. 20 strings with variable length were hung over the edge of the cage. Half of the strings were baited with chocolate flavored sucrose pellets. Mice were removed from the apparatus once all of the strings had been pulled into the cage, or once 20 minutes had elapsed. On subsequent days 2 and 3, mice were again placed in the cage with 20 strings to pull. Following this 3-day habituation, from days 4-14 mice were habituated in an alternate transparent string pull box with high sides and transparent front face for video recording. Within this second habituation box, mice received 3 trials with baited strings hung facing the recording camera. The session was terminated when the animal had pulled all three strings or once 20 minutes had elapsed, and the apparatus prepared for the next mouse. On the last day prior to the first Ca^{2+} imaging session, 3 trials of string pull from each mouse were recorded with the use of a GoPro Hero 7 Black (60 fps, 1920×1080 pixels). Mice were re-tested with this same 3 string protocol the day prior to each of their weekly imaging timepoints. Video recordings were analyzed using a semi-automated Matlab string pull package [141]. Reach and withdraw movement scaling for the left and right paw was calculated by running a Pearson's correlation between the series of Euclidian distances that the paw travelled during each of the reach or withdraw movements during the string pull and correlating with the peak speed of the paw during each of the respective reaches or withdraws [142]. A value of 1 indicates a strong linear relationship between longer reach/withdraw paw movement distance and greater peak speed that the paw obtained. Paw reach distance was calculated as the average distance that the paw travelled during each reach movement. Path circuity is used as a measure of how direct of a path a reach or withdraw movement takes between its starting and end points and is calculated as the total distance travelled divided by the

Euclidian distance between the start and end points [142]. The greater the path circuity value is above 1, the more the path of the paw deviated from the ideal direct path between the start and end points of the reach/withdraw. A bimanual correlation coefficient was calculated by first detrending the timeseries of Y-axis paw position to remove general changes in the posture of the animal over the course of the string pull attempt, then running a Pearson's correlation between the Y-axis paw position measurements for the right and left paw.

Mobile floating homecage habituation and measurement of movement parameters

Methods for floating homecage (Neurotar, Finland) habituation have previously been described [143], with modification as follows. 2-weeks after cranial window implantation, each mouse was handled for 5 minutes 3 times per day for the first 2 days to habituate them to handling. For days 3-4, each mouse was handled and repeatedly wrapped and released with a soft cloth for a period of 5 mins 3 times per day in order to habituate to the wrapping procedure. Mice were also given 1 period of 5 minutes each per day to freely explore the floating homecage without being head-restrained. For days 5-8, twice per day the animals were head-restrained in the floating homecage and allowed to move around the floating homecage for a period of 15 minutes with the room lights off before being returned to their cage. For days 8-14, twice per day the mice were head-restrained in the floating homecage for 25 minutes with the floating homecage attached to the microscope in the same conditions in which the animals would be imaged on day 15 onwards. On day 14 (one day prior to their first imaging session) baseline performance on the string pull and tapered beam tasks was measured prior to their last habituation in the floating homecage. Animal movement within the homecage during each Ca^{2+} imaging sessions was tracked to determine animal speed and position. Movement periods were

manually annotated on a subset of timeseries by co-recording animal movement using both the Mobile Homecage tracker, as well as a webcam (Logitech C270) with infrared filter removed. Movement tracking data was low pass filtered to remove spurious movement artifacts lasting below 6 recording frames (240ms). Based on annotated times of animal movement from the webcam recordings and Homecage tracking, a threshold of 30mm/s from the tracking data was determined as frames of animal movement, whereas speeds below 30mm/s were taken as periods of rest.

Identification of forelimb and hindlimb somatosensory cortex representations using widefield Ca^{2+} imaging of sensory-evoked responses

On day 10 of habituation, mice were anesthetized with 1.25% isofluorane after they had completed all daily task training and floating homecage habituation. Mice were head-fixed on a stereotaxic frame with continuous isofluorane anesthesia. Body temperature was measured using a rectal probe and maintained at 37±0.5^{o}C. The cortical surface was illuminated with blue light from a xenon lamp (excitation band-pass filtered at 450-490nm). Fluorescent emissions were long-pass filtered at 515nm and captured in 12-bit format by a Dalsa Pantera 1M60 camera mounted on a Leica SP5 confocal microscope using a 2.5X objective. The depth of focus was set at 200 μm below the cortical surface. Custom-made piezoceramic mechanical bending actuators were used to elicit oscillatory limb stimulation during widefield Ca^{2+} imaging. The piezo bending actuators comprised a piezo element (Piezo Systems # Q220-A4-203YB) attached to an electrically insulated metal shaft holding a metal U-bend at its end. The palm of the mouse paw was placed within the U-bend, and the U-bend bent to shape to lightly secure the palm. The metal U-bend made contact across a vertical rectangular area of approximately 3x1mm on the

palmar and dorsal surface of the hand. Stimulators were driven with square-wave signals from an A-M Systems Model 2100 Isolated Pulse Stimulator. Stimulation alternated between contralateral forelimb (cFL) and contralateral hindlimb (cHL) for up to 40 trials of stimulation of each limb. Placement of actuators was on the glabrous skin of the forepaw or hindpaw, with consistent alignment relative to the flexion of wrist and ankle. Images were captured for 5.0s at 10 Hz (1s before and 4s after stimulus onset; interstimulus interval = 20s). The trials for each limb were averaged in ImageJ software (NIH). 10 imaging frames (1s) after stimulus onset were averaged and divided by the 10 baseline frames 1s before stimulus onset to generate a response map for each limb. Response maps were thresholded at 5 times the standard deviation of the baseline period deltaFoF to determine limb associated response maps. These were merged and overlaid on an image of surface vasculature to delineate the cFL and cHL somatosensory representations and were also used to determine peak Ca^{2+} response amplitude from the timeseries recordings. For cFL stimulation trials, an additional ROI was placed over the region lateral to the cHL representation (denoted as “distal region” in Fig 2E) to measure the distal region cFL evoked Ca^{2+} response amplitude pre- and post-stroke. The dimensions and position of the distal ROI was held consistent relative to surface vasculature for each animal from pre- to post-stroke.

Calcium imaging

On the day following testing for behavioral performance on the string pull and tapered beam tasks, animals were head-fixed within the mobile homecage and Ca^{2+} imaging was performed. Awake in-vivo two-photon imaging was performed using a Leica SP5 MP confocal microscope equipped with a Ti:Sapphire Coherent Chameleon Vision II laser tuned to 940 nm

for GCaMP6S excitation. A Leica HCX PL APO L 20x 1.0NA water immersion objective was used. Images were acquired using Leica LAS AF using no averaging, a zoom of 1.7x and a frame -rate of 25Hz. Images were acquired at 512x512 pixels over an area of 434x434μm, yielding a resolution of 0.848μm per pixel. Two imaging regions were chosen for each animal, with one corresponding to the half-way point between the pre-stroke cFL and cHL somatosensory maps previously determined with widefield Ca^{2+} imaging (the "peri-infarct" imaging region), and the other an imaging region located just lateral to the cHL sensory map (the "distal" imaging region). These regions can be seen in Fig 1D and Fig 2A. Each imaging region was recorded for 15 minutes while simultaneously tracking the animal's movement and position within the mobile homecage. Imaging depth was set between 100-180um below the cortical surface. There were no differences between the stroke group and sham group for movement within the mobile homecage, though both groups displayed an equivalent decrease in the amount of time they spent moving within the 15 minute recording sessions over the course of the 8-week experimental timeline, potentially reflecting continuing habituation over this period.

Photothrombotic stroke and sham procedure

After baseline cellular Ca^{2+} imaging, mice were anesthetized using 1.25% isofluorane and head-fixed on a stereotaxic frame with continuous isofluorane anesthesia. Body temperature was measured using a rectal probe and maintained at 37±0.5^{o}C. The mapped cFL area was used as a guide for a targeted photothrombosis procedure. Briefly, a 2mm diameter hole was punched in black electrical tape and attached onto the glass window to block stray light from illuminating cortical areas outside of the desired region. Rose Bengal (a photosensitive dye) was dissolved in 0.01M sterile phosphate buffered saline (Sigma) and injected intraperitoneal (30mg/kg). The cFL

cortical area visible through the punched electrical tape was illuminated using a collimated beam of green laser light (532 nm, 17mW) for 20 minutes to photoactivate the Rose Bengal and cause a focal ischemic lesion. Sham controls were treated in the same manner as stroke, however illumination of the laser was omitted.

Two-photon image processing and analysis of neuronal activity

Timeseries images (15 minutes per imaging region, 22500 frames per recording, 25fps) were group averaged in groups of 2, then motion corrected using the TurboReg plugin in FiJi with translation only registration [144]. Z-projections within FiJi of the average and standard deviation were used to define neuronal ROI through manual tracing. Using custom written scripts in Matlab 2020b, ROIs were imported and converted into a format suitable for the Ca^{2+} imaging toolbox used for subsequent steps [59]. Neuropil for each ROI was determined by expanding an annular donut around each ROI to calculate the neuropil deltaF/Fo surrounding each ROI. During computation of neuron ROI deltaF/Fo, fluorescence was corrected for neuropil contamination using the formula ($F_{corrected} = F_{raw} – \alpha * F_{neuropil}$) where α was set to 0.4 based on previous studies suggesting that α values between 0.3-0.5 were optimal [145], and with $F_{neuropil}$ determined by the peri-somatic donut neuropil fluorescence closely associated with each neuron. A smoothed estimate of the baseline fluorescence was calculated by taking a 30s running average of the 8th percentile of the raw fluorescence, which was then subtracted from the raw fluorescence to remove baseline drift.

Ca^{2+} trace deconvolution to determine neuronal transients

To determine significant fluorescent Ca^{2+} transients from the deltaF/Fo of each neuron, a

dynamic threshold implementing a Bayesian odds ratio estimation framework for noise estimation was used to determine transients that met the condition of being greater than 98% of the confidence interval for the calculated fluorescent baseline noise, and were compatible with a tau of ~1.8s for GCaMP6S [58,59]. Determination of firing was performed on the neuronal deltaF/Fo traces, as implemented in [58,59], in order to define the Ca^{2+} transient rate and to generate raster plots. This information was used to determine neuronal activity "firing rate" as shown in Fig 4.

Neuron-neuron correlation analysis and functional connectivity

Using custom written scripts in Matlab, Pearson product-moment correlation coefficients were calculated between the z-scored Ca^{2+} traces derived from each of the neuronal ROIs in a given optical section. Distance between neuron pairs was calculated from the Euclidean distance between the central points of the neuron ROIs of the image frame. Functional connectivity plots (Fig 5) were generated by plotting neuron ROI centroids as red dots, and lines between them with line weight and color determined by the strength of the correlation between them. Stationary variable block bootstrapping (5000 iterations) was performed as a statistical test for the significance of each pairwise correlation and only correlations that were greater than the 99th percentile of the bootstrap were deemed statistically significant and plotted. Average number of significant connections per neuron was calculated by dividing the number of functional connections that met the bootstrapping threshold by the total number of neurons in the population. Connection density was calculated as percent of max by taking the total number of significant functional connections and dividing by the total potential number of functional connections if every neuron within the population was functionally connected with all other

neurons.

Determination of neural assemblies and their activity patterns

To evaluate the co-activity patterns of neurons that form putative neural assemblies, a PCA-Promax procedure was applied as previously described [58,59], with a zMax threshold manually selected by the first clear minimum in the distribution of z-scored maximal ROI loadings. Notably, the PCA-Promax procedure relaxes the PCA orthogonality condition using a PROMAX oblique rotation of the PC axes [146], such that assemblies can contain neurons found within other assemblies. Due to this relaxation of the PCA orthogonality condition, assemblies with high overlap whose dot product exceeded 0.6 were merged [146]. All assemblies were compared to surrogate control datasets, and only those assemblies whose members were significantly correlated and synchronous were kept ($p < 0.05$). To determine the co-activity of neurons within assemblies, a matching index was calculated [58,59,147,148]. The matching index quantifies the proportion of neurons within the assembly that are co-activated simultaneously over the timeseries, with a maximal value of 1 indicating perfect overlap in assembly member activation. The significance of each assembly activation over the timeseries was determined by comparing the activation events to a probability distribution based on the size of the assembly, the size of the total population of N ROIs, and with a threshold p-value of <0.05 considered to be a statistically significant activation. For cross-correlation of assembly activations with speed (Fig S3) and assembly-assembly correlations (Fig 9), the matching index was first multiplied by the Boolean timeseries of individual assembly activation significance to generate matching index timeseries of significant assembly activations only (presented in Fig S3 and Fig 9 as percent of maximal assembly activation). ROIs of assembly members were color

coded according to their assembly membership, and overlaid on an averaged fluorescence image to generate assembly plots (Fig 7).

Statistical analysis

Multivariate comparisons were made using a mixed-effects model for repeated measures based on a restricted maximum likelihood generalized linear mixed model as implemented in Graphpad Prism 9.0.0, with Bonferroni-Sidak corrections used for *post-hoc* comparisons. Bonferroni-Sidak *post-hoc* testing was used to compare the means of the stroke vs. the sham group at each timepoint, as well as to identify within group differences by comparing different timepoints within each group. Grubb's test was used to remove data outliers with alpha set to 0.05. All zero time-lag cross-correlations were computed using Pearson's *r*. A stationary bootstrapping procedure was used as a test of the significance of the calculated Pearson's r of each pairwise timeseries comparison. Within the stationary bootstrapping procedure, 5000 iterations were run and an average block length of 23 frames (1.84s) was used based on previous studies indicating ~1.8s as the decay time for GCaMP6S Ca^{2+} sensor within neurons [149,150]. Pairwise r values greater than the 99th percentile of the stationary bootstrap were deemed 'significant'. Non-significant pairwise r values were excluded from analyses of average correlation values. For all statistical comparisons, a *p* value of ≤0.05 was considered statistically significant. A *p* value of ≤0.10 was considered a statistical trend. Data are expressed as the mean ± SEM.

Author Contributions

MVB and IRW designed all experiments. MVB performed experiments and analyzed data. MVB and IRW wrote the manuscript together.

Competing Interests

The authors declare no competing interests.

Data Availability

All data generated or analyzed during this study has been made publicly available on OSF (https://osf.io/wam9j/).

REFERENCES

1. Schiene K, Bruehl C, Zilles K, Qü M, Hagemann G, Kraemer M, et al. Neuronal hyperexcitability and reduction of GABAA-receptor expression in the surround of cerebral photothrombosis. J Cereb Blood Flow Metab Off J Int Soc Cereb Blood Flow Metab. 1996;16: 906–914. doi:10.1097/00004647-199609000-00014

2. Mittmann T, Qü M, Zilles K, Luhmann HJ. Long-term cellular dysfunction after focal cerebral ischemia: in vitro analyses. Neuroscience. 1998;85: 15–27. doi:10.1016/S0306-4522(97)00638-6

3. Neumann-Haefelin T, Staiger JF, Redecker C, Zilles K, Fritschy JM, Möhler H, et al. Immunohistochemical evidence for dysregulation of the GABAergic system ipsilateral to photochemically induced cortical infarcts in rats. Neuroscience. 1998;87: 871–879. doi:10.1016/s0306-4522(98)00124-9

4. Neumann-Haefelin T, Bosse F, Redecker C, Müller HW, Witte OW. Upregulation of GABAA-receptor alpha1- and alpha2-subunit mRNAs following ischemic cortical lesions in rats. Brain Res. 1999;816: 234–237. doi:10.1016/s0006-8993(98)01162-7

5. Qü M, Buchkremer-Ratzmann I, Schiene K, Schroeter M, Witte OW, Zilles K. Bihemispheric reduction of GABAA receptor binding following focal cortical photothrombotic lesions in the rat brain. Brain Res. 1998;813: 374–380. doi:10.1016/s0006-8993(98)01063-4

6. Redecker C, Wang W, Fritschy J-M, Witte OW. Widespread and Long-Lasting Alterations in GABAA-Receptor Subtypes after Focal Cortical Infarcts in Rats: Mediation by NMDA-Dependent Processes. J Cereb Blood Flow Metab. 2002;22: 1463–1475. doi:10.1097/01.WCB.0000034149.72481.BD

7. Luhmann HJ, Mudrick-Donnon LA, Mittmann T, Heinemann U. Ischaemia-induced long-term hyperexcitability in rat neocortex. Eur J Neurosci. 1995;7: 180–191. doi:10.1111/j.1460-9568.1995.tb01054.x

8. Buchkremer-Ratzmann I, Witte OW. Extended brain disinhibition following small photothrombotic lesions in rat frontal cortex. NeuroReport. 1997;8: 519–522.

9. Domann R, Hagemann G, Kraemer M, Freund H-J, Witte OW. Electrophysiological changes in the surrounding brain tissue of photochemically induced cortical infarcts in the rat. Neurosci Lett. 1993;155: 69–72. doi:10.1016/0304-3940(93)90675-B

10. Fujioka H, Kaneko H, Suzuki SS, Mabuchi K. Hyperexcitability-associated rapid plasticity after a focal cerebral ischemia. Stroke. 2004;35: e346-348. doi:10.1161/01.STR.0000130990.28734.9c

11. Qü M, Mittmann T, Luhmann HJ, Schleicher A, Zilles K. Long-term changes of

ionotropic glutamate and GABA receptors after unilateral permanent focal cerebral ischemia in the mouse brain. Neuroscience. 1998;85: 29–43. doi:10.1016/s0306-4522(97)00656-8

12. Que M, Schiene K, Witte OW, Zilles K. Widespread up-regulation of N-methyl-D-aspartate receptors after focal photothrombotic lesion in rat brain. Neurosci Lett. 1999;273: 77–80. doi:10.1016/s0304-3940(99)00598-4

13. Jaenisch N, Liebmann L, Guenther M, Hübner CA, Frahm C, Witte OW. Reduced tonic inhibition after stroke promotes motor performance and epileptic seizures. Sci Rep. 2016;6: 26173. doi:10.1038/srep26173

14. Jin X, Huguenard JR, Prince DA. Impaired Cl- extrusion in layer V pyramidal neurons of chronically injured epileptogenic neocortex. J Neurophysiol. 2005;93: 2117–2126. doi:10.1152/jn.00728.2004

15. Khirug S, Soni S, Saez Garcia M, Tessier M, Zhou L, Kulesskaya N, et al. Protective Role of Low Ethanol Administration Following Ischemic Stroke via Recovery of KCC2 and p75NTR Expression. Mol Neurobiol. 2021;58: 1145–1161. doi:10.1007/s12035-020-02176-x

16. Martín-Aragón Baudel MAS, Poole AV, Darlison MG. Chloride co-transporters as possible therapeutic targets for stroke. J Neurochem. 2017;140: 195–209. doi:10.1111/jnc.13901

17. Schulte JT, Wierenga CJ, Bruining H. Chloride transporters and GABA polarity in developmental, neurological and psychiatric conditions. Neurosci Biobehav Rev. 2018;90: 260–271. doi:10.1016/j.neubiorev.2018.05.001

18. Witte OW, Freund HJ. Neuronal dysfunction, epilepsy, and postlesional brain plasticity. Adv Neurol. 1999;81: 25–36.

19. Brown CE, Aminoltejari K, Erb H, Winship IR, Murphy TH. In Vivo Voltage-Sensitive Dye Imaging in Adult Mice Reveals That Somatosensory Maps Lost to Stroke Are Replaced over Weeks by New Structural and Functional Circuits with Prolonged Modes of Activation within Both the Peri-Infarct Zone and Distant Sites. J Neurosci. 2009;29: 1719–1734. doi:10.1523/JNEUROSCI.4249-08.2009

20. Chen S, Mohajerani MH, Xie Y, Murphy TH. Optogenetic analysis of neuronal excitability during global ischemia reveals selective deficits in sensory processing following reperfusion in mouse cortex. J Neurosci Off J Soc Neurosci. 2012;32: 13510–13519. doi:10.1523/JNEUROSCI.1439-12.2012

21. Lim DH, LeDue JM, Mohajerani MH, Murphy TH. Optogenetic mapping after stroke reveals network-wide scaling of functional connections and heterogeneous recovery of the peri-infarct. J Neurosci Off J Soc Neurosci. 2014;34: 16455–16466.

doi:10.1523/JNEUROSCI.3384-14.2014

22. Sigler A, Mohajerani MH, Murphy TH. Imaging rapid redistribution of sensory-evoked depolarization through existing cortical pathways after targeted stroke in mice. Proc Natl Acad Sci. 2009;106: 11759–11764.

23. Sweetnam DA, Brown CE. Stroke induces long-lasting deficits in the temporal fidelity of sensory processing in the somatosensory cortex. J Cereb Blood Flow Metab Off J Int Soc Cereb Blood Flow Metab. 2013;33: 91–96. doi:10.1038/jcbfm.2012.135

24. Sweetnam D, Holmes A, Tennant KA, Zamani A, Walle M, Jones P, et al. Diabetes Impairs Cortical Plasticity and Functional Recovery Following Ischemic Stroke. J Neurosci. 2012;32: 5132–5143. doi:10.1523/JNEUROSCI.5075-11.2012

25. Winship IR, Murphy TH. In vivo calcium imaging reveals functional rewiring of single somatosensory neurons after stroke. J Neurosci Off J Soc Neurosci. 2008;28: 6592–6606. doi:10.1523/JNEUROSCI.0622-08.2008

26. Cramer JV, Gesierich B, Roth S, Dichgans M, Düring M, Liesz A. In vivo widefield calcium imaging of the mouse cortex for analysis of network connectivity in health and brain disease. NeuroImage. 2019;199: 570–584. doi:10.1016/j.neuroimage.2019.06.014

27. Grandjean J, Schroeter A, Batata I, Rudin M. Optimization of anesthesia protocol for resting-state fMRI in mice based on differential effects of anesthetics on functional connectivity patterns. NeuroImage. 2014;102: 838–847. doi:10.1016/j.neuroimage.2014.08.043

28. Jonckers E, Delgado y Palacios R, Shah D, Guglielmetti C, Verhoye M, Van der Linden A. Different anesthesia regimes modulate the functional connectivity outcome in mice. Magn Reson Med. 2014;72: 1103–1112. doi:10.1002/mrm.24990

29. Kalthoff D, Po C, Wiedermann D, Hoehn M. Reliability and spatial specificity of rat brain sensorimotor functional connectivity networks are superior under sedation compared with general anesthesia. NMR Biomed. 2013;26: 638–650. doi:10.1002/nbm.2908

30. Nasrallah FA, Tay H-C, Chuang K-H. Detection of functional connectivity in the resting mouse brain. NeuroImage. 2014;86: 417–424. doi:10.1016/j.neuroimage.2013.10.025

31. Chapin JK, Lin CS. Mapping the body representation in the SI cortex of anesthetized and awake rats. J Comp Neurol. 1984;229: 199–213. doi:10.1002/cne.902290206

32. Chen LM, Friedman RM, Roe AW. Optical imaging of SI topography in anesthetized and awake squirrel monkeys. J Neurosci Off J Soc Neurosci. 2005;25: 7648–7659. doi:10.1523/JNEUROSCI.1990-05.2005

33. Devonshire IM, Grandy TH, Dommett EJ, Greenfield SA. Effects of urethane anaesthesia on sensory processing in the rat barrel cortex revealed by combined optical imaging and

electrophysiology. Eur J Neurosci. 2010;32: 786–797. doi:10.1111/j.1460-9568.2010.07322.x

34. Lissek T, Obenhaus HA, Ditzel DAW, Nagai T, Miyawaki A, Sprengel R, et al. General Anesthetic Conditions Induce Network Synchrony and Disrupt Sensory Processing in the Cortex. Front Cell Neurosci. 2016;10: 64. doi:10.3389/fncel.2016.00064

35. Ebner FF, Kaas JH. Chapter 24 - Somatosensory System. In: Paxinos G, editor. The Rat Nervous System (Fourth Edition). San Diego: Academic Press; 2015. pp. 675–701. doi:10.1016/B978-0-12-374245-2.00024-3

36. Friedberg MH, Lee SM, Ebner FF. Modulation of Receptive Field Properties of Thalamic Somatosensory Neurons by the Depth of Anesthesia. J Neurophysiol. 1999;81: 2243–2252. doi:10.1152/jn.1999.81.5.2243

37. Faggin BM, Nguyen KT, Nicolelis MA. Immediate and simultaneous sensory reorganization at cortical and subcortical levels of the somatosensory system. Proc Natl Acad Sci U S A. 1997;94: 9428–9433. doi:10.1073/pnas.94.17.9428

38. Moore CI, Nelson SB. Spatio-Temporal Subthreshold Receptive Fields in the Vibrissa Representation of Rat Primary Somatosensory Cortex. J Neurophysiol. 1998;80: 2882–2892. doi:10.1152/jn.1998.80.6.2882

39. Nicolelis MA, Chapin JK. Spatiotemporal structure of somatosensory responses of many-neuron ensembles in the rat ventral posterior medial nucleus of the thalamus. J Neurosci. 1994;14: 3511–3532. doi:10.1523/JNEUROSCI.14-06-03511.1994

40. Crapse TB, Sommer MA. Corollary discharge across the animal kingdom. Nat Rev Neurosci. 2008;9: 587–600. doi:10.1038/nrn2457

41. Afrashteh N, Inayat S, Bermudez-Contreras E, Luczak A, McNaughton BL, Mohajerani MH. Spatiotemporal structure of sensory-evoked and spontaneous activity revealed by mesoscale imaging in anesthetized and awake mice. Cell Rep. 2021;37: 110081. doi:10.1016/j.celrep.2021.110081

42. Dionne JK, Legon W, Staines WR. Crossmodal influences on early somatosensory processing: interaction of vision, touch, and task-relevance. Exp Brain Res. 2013;226: 503–512. doi:10.1007/s00221-013-3462-z

43. Johansen-Berg H, Christensen V, Woolrich M, Matthews PM. Attention to touch modulates activity in both primary and secondary somatosensory areas. Neuroreport. 2000;11: 1237–1241.

44. Nelson AJ, Staines WR, Graham SJ, McIlroy WE. Activation in SI and SII: the influence of vibrotactile amplitude during passive and task-relevant stimulation. Brain Res Cogn Brain Res. 2004;19: 174–184. doi:10.1016/j.cogbrainres.2003.11.013

45. Staines WR, Graham SJ, Black SE, McIlroy WE. Task-relevant modulation of contralateral and ipsilateral primary somatosensory cortex and the role of a prefrontal-cortical sensory gating system. NeuroImage. 2002;15: 190–199. doi:10.1006/nimg.2001.0953

46. Gomez-Ramirez M, Hysaj K, Niebur E. Neural mechanisms of selective attention in the somatosensory system. J Neurophysiol. 2016;116: 1218–1231. doi:10.1152/jn.00637.2015

47. Scaglione A, Foffani G, Moxon KA. Spike count, spike timing and temporal information in the cortex of awake, freely moving rats. J Neural Eng. 2014;11: 046022. doi:10.1088/1741-2560/11/4/046022

48. Yu J, Gutnisky DA, Hires SA, Svoboda K. Layer 4 fast-spiking interneurons filter thalamocortical signals during active somatosensation. Nat Neurosci. 2016;19: 1647–1657. doi:10.1038/nn.4412

49. London BM, Miller LE. Responses of somatosensory area 2 neurons to actively and passively generated limb movements. J Neurophysiol. 2013;109: 1505–1513. doi:10.1152/jn.00372.2012

50. Nelson RJ. Activity of monkey primary somatosensory cortical neurons changes prior to active movement. Brain Res. 1987;406: 402–407. doi:10.1016/0006-8993(87)90815-8

51. Bensmaia S, Helms Tillery SI. Tactile Feedback from the Hand. In: Balasubramanian R, Santos VJ, editors. The Human Hand as an Inspiration for Robot Hand Development. Cham: Springer International Publishing; 2014. pp. 143–157. doi:10.1007/978-3-319-03017-3_7

52. Winship IR, Murphy TH. Remapping the somatosensory cortex after stroke: insight from imaging the synapse to network. Neurosci Rev J Bringing Neurobiol Neurol Psychiatry. 2009;15: 507–524. doi:10.1177/1073858409333076

53. Ardesch DJ, Balbi M, Murphy TH. Automated touch sensing in the mouse tapered beam test using Raspberry Pi. J Neurosci Methods. 2017;291: 221–226. doi:10.1016/j.jneumeth.2017.08.030

54. Zhao C, Puurunen K, Schallert T, Sivenius J, Jolkkonen J. Effect of cholinergic medication, before and after focal photothrombotic ischemic cortical injury, on histological and functional outcome in aged and young adult rats. Behav Brain Res. 2005;156: 85–94. doi:10.1016/j.bbr.2004.05.011

55. Lipsanen A, Hiltunen M, Jolkkonen J. Chronic ibuprofen treatment does not affect the secondary pathology in the thalamus or improve behavioral outcome in middle cerebral artery occlusion rats. Pharmacol Biochem Behav. 2011;99: 468–474. doi:10.1016/j.pbb.2011.04.019

56. Schallert T, Woodlee MT, Fleming SM. Disentangling multiple types of recovery from

brain injury. Pharmacol Cereb Ischemia. 2002; 201–216.

57. Blackwell AA, Widick WL, Cheatwood JL, Whishaw IQ, Wallace DG. Unilateral forelimb sensorimotor cortex devascularization disrupts the topographic and kinematic characteristics of hand movements while string-pulling for food in the rat. Behav Brain Res. 2018;338: 88–100. doi:10.1016/j.bbr.2017.10.014

58. Romano SA, Pietri T, Pérez-Schuster V, Jouary A, Haudrechy M, Sumbre G. Spontaneous Neuronal Network Dynamics Reveal Circuit's Functional Adaptations for Behavior. Neuron. 2015;85: 1070–1085. doi:10.1016/j.neuron.2015.01.027

59. Romano SA, Pérez-Schuster V, Jouary A, Boulanger-Weill J, Candeo A, Pietri T, et al. An integrated calcium imaging processing toolbox for the analysis of neuronal population dynamics. PLoS Comput Biol. 2017;13: e1005526. doi:10.1371/journal.pcbi.1005526

60. Zeiger WA, Marosi M, Saggi S, Noble N, Samad I, Portera-Cailliau C. Barrel cortex plasticity after photothrombotic stroke involves potentiating responses of pre-existing circuits but not functional remapping to new circuits. Nat Commun. 2021;12: 3972. doi:10.1038/s41467-021-24211-8

61. Motaharinia M, Gerrow K, Boghozian R, White E, Choi S-E, Delaney KR, et al. Longitudinal functional imaging of VIP interneurons reveals sup-population specific effects of stroke that are rescued with chemogenetic therapy. Nat Commun. 2021;12: 6112. doi:10.1038/s41467-021-26405-6

62. Bauer AQ, Kraft AW, Wright PW, Snyder AZ, Lee J-M, Culver JP. Optical imaging of disrupted functional connectivity following ischemic stroke in mice. NeuroImage. 2014;99: 388–401. doi:10.1016/j.neuroimage.2014.05.051

63. Blaschke SJ, Hensel L, Minassian A, Vlachakis S, Tscherpel C, Vay SU, et al. Translating Functional Connectivity After Stroke: Functional Magnetic Resonance Imaging Detects Comparable Network Changes in Mice and Humans. Stroke. 2021;52: 2948–2960. doi:10.1161/STROKEAHA.120.032511

64. Carter AR, Astafiev SV, Lang CE, Connor LT, Rengachary J, Strube MJ, et al. Resting interhemispheric functional magnetic resonance imaging connectivity predicts performance after stroke. Ann Neurol. 2010;67: 365–375. doi:10.1002/ana.21905

65. Carter AR, Shulman GL, Corbetta M. Why use a connectivity-based approach to study stroke and recovery of function? NeuroImage. 2012;62: 2271–2280. doi:10.1016/j.neuroimage.2012.02.070

66. Hakon J, Quattromani MJ, Sjölund C, Tomasevic G, Carey L, Lee J-M, et al. Multisensory stimulation improves functional recovery and resting-state functional connectivity in the mouse brain after stroke. NeuroImage Clin. 2017;17: 717–730. doi:10.1016/j.nicl.2017.11.022

67. Longo V, Barbati SA, Re A, Paciello F, Bolla M, Rinaudo M, et al. Transcranial Direct Current Stimulation Enhances Neuroplasticity and Accelerates Motor Recovery in a Stroke Mouse Model. Stroke. 2022; STROKEAHA121034200. doi:10.1161/STROKEAHA.121.034200

68. Olafson ER, Jamison KW, Sweeney EM, Liu H, Wang D, Bruss JE, et al. Functional connectome reorganization relates to post-stroke motor recovery and structural and functional disconnection. NeuroImage. 2021;245: 118642. doi:10.1016/j.neuroimage.2021.118642

69. Rehme AK, Grefkes C. Cerebral network disorders after stroke: evidence from imaging-based connectivity analyses of active and resting brain states in humans. J Physiol. 2013;591: 17–31. doi:10.1113/jphysiol.2012.243469

70. Siegel JS, Ramsey LE, Snyder AZ, Metcalf NV, Chacko RV, Weinberger K, et al. Disruptions of network connectivity predict impairment in multiple behavioral domains after stroke. Proc Natl Acad Sci U S A. 2016;113: E4367–E4376. doi:10.1073/pnas.1521083113

71. Silasi G, Murphy TH. Stroke and the Connectome: How Connectivity Guides Therapeutic Intervention. Neuron. 2014;83: 1354–1368. doi:10.1016/j.neuron.2014.08.052

72. Urbin MA, Hong X, Lang CE, Carter AR. Resting-state functional connectivity and its association with multiple domains of upper-extremity function in chronic stroke. Neurorehabil Neural Repair. 2014;28: 761–769. doi:10.1177/1545968314522349

73. Latifi S, Mitchell S, Habibey R, Hosseini F, Donzis E, Estrada-Sánchez AM, et al. Neuronal Network Topology Indicates Distinct Recovery Processes after Stroke. Cereb Cortex N Y NY. 2020;30: 6363–6375. doi:10.1093/cercor/bhaa191

74. Bechay KR, Abduljawad N, Latifi S, Suzuki K, Iwashita H, Carmichael ST. PDE2A Inhibition Enhances Axonal Sprouting, Functional Connectivity, and Recovery after Stroke. J Neurosci. 2022;42: 8225–8236. doi:10.1523/JNEUROSCI.0730-22.2022

75. Buzsáki G. Neural syntax: cell assemblies, synapsembles, and readers. Neuron. 2010;68: 362–385. doi:10.1016/j.neuron.2010.09.023

76. Buzsáki G, Watson BO. Brain rhythms and neural syntax: implications for efficient coding of cognitive content and neuropsychiatric disease. Dialogues Clin Neurosci. 2012;14: 345–367. doi:10.31887/DCNS.2012.14.4/gbuzsaki

77. Palm G, Knoblauch A, Hauser F, Schüz A. Cell assemblies in the cerebral cortex. Biol Cybern. 2014;108: 559–572. doi:10.1007/s00422-014-0596-4

78. Mölter J, Avitan L, Goodhill GJ. Detecting neural assemblies in calcium imaging data. BMC Biol. 2018;16: 143. doi:10.1186/s12915-018-0606-4

79. Deolindo CS, Kunicki ACB, da Silva MI, Lima Brasil F, Moioli RC. Neuronal Assemblies Evidence Distributed Interactions within a Tactile Discrimination Task in Rats. Front Neural Circuits. 2017;11: 114. doi:10.3389/fncir.2017.00114

80. Murphy TH, Corbett D. Plasticity during stroke recovery: from synapse to behaviour. Nat Rev Neurosci. 2009;10: 861–872. doi:10.1038/nrn2735

81. Xu X, Ye L, Ruan Q. Environmental enrichment induces synaptic structural modification after transient focal cerebral ischemia in rats. Exp Biol Med Maywood NJ. 2009;234: 296–305. doi:10.3181/0804-RM-128

82. Biernaskie J, Chernenko G, Corbett D. Efficacy of rehabilitative experience declines with time after focal ischemic brain injury. J Neurosci Off J Soc Neurosci. 2004;24: 1245–1254. doi:10.1523/JNEUROSCI.3834-03.2004

83. Brown CE, Li P, Boyd JD, Delaney KR, Murphy TH. Extensive turnover of dendritic spines and vascular remodeling in cortical tissues recovering from stroke. J Neurosci Off J Soc Neurosci. 2007;27: 4101–4109. doi:10.1523/JNEUROSCI.4295-06.2007

84. Carmichael ST, Archibeque I, Luke L, Nolan T, Momiy J, Li S. Growth-associated gene expression after stroke: evidence for a growth-promoting region in peri-infarct cortex. Exp Neurol. 2005;193: 291–311. doi:10.1016/j.expneurol.2005.01.004

85. Cheatwood JL, Emerick AJ, Kartje GL. Neuronal plasticity and functional recovery after ischemic stroke. Top Stroke Rehabil. 2008;15: 42–50. doi:10.1310/tsr1501-42

86. Ploughman M, Windle V, MacLellan CL, White N, Doré JJ, Corbett D. Brain-derived neurotrophic factor contributes to recovery of skilled reaching after focal ischemia in rats. Stroke. 2009;40: 1490–1495. doi:10.1161/STROKEAHA.108.531806

87. Carmichael ST. Plasticity of Cortical Projections after Stroke. The Neuroscientist. 2003;9: 64–75. doi:10.1177/1073858402239592

88. Carmichael ST. Cellular and molecular mechanisms of neural repair after stroke: Making waves. Ann Neurol. 2006;59: 735–742. doi:10.1002/ana.20845

89. Dancause N. Extensive Cortical Rewiring after Brain Injury. J Neurosci. 2005;25: 10167–10179. doi:10.1523/JNEUROSCI.3256-05.2005

90. Carmichael ST. Gene expression changes after focal stroke, traumatic brain and spinal cord injuries. Curr Opin Neurol. 2003;16: 699–704. doi:10.1097/01.wco.0000102621.38669.77

91. Li S, Carmichael ST. Growth-associated gene and protein expression in the region of axonal sprouting in the aged brain after stroke. Neurobiol Dis. 2006;23: 362–373. doi:10.1016/j.nbd.2006.03.011

92. Li S, Overman JJ, Katsman D, Kozlov SV, Donnelly CJ, Twiss JL, et al. An age-related sprouting transcriptome provides molecular control of axonal sprouting after stroke. Nat Neurosci. 2010;13: 1496–1504. doi:10.1038/nn.2674

93. Paz JT, Christian CA, Parada I, Prince DA, Huguenard JR. Focal cortical infarcts alter intrinsic excitability and synaptic excitation in the reticular thalamic nucleus. J Neurosci Off J Soc Neurosci. 2010;30: 5465–5479. doi:10.1523/JNEUROSCI.5083-09.2010

94. Staines WR, Black SE, Graham SJ, McIlroy WE. Somatosensory gating and recovery from stroke involving the thalamus. Stroke. 2002;33: 2642–2651. doi:10.1161/01.str.0000032552.40405.40

95. Carmichael ST, Wei L, Rovainen CM, Woolsey TA. New patterns of intracortical projections after focal cortical stroke. Neurobiol Dis. 2001;8: 910–922. doi:10.1006/nbdi.2001.0425

96. Tennant KA, Taylor SL, White ER, Brown CE. Optogenetic rewiring of thalamocortical circuits to restore function in the stroke injured brain. Nat Commun. 2017;8: 15879. doi:10.1038/ncomms15879

97. Brown CE, Murphy TH. Livin' on the Edge: Imaging Dendritic Spine Turnover in the Peri -Infarct Zone during Ischemic Stroke and Recovery. The Neuroscientist. 2008;14: 139–146. doi:10.1177/1073858407309854

98. Ergul A, Alhusban A, Fagan SC. Angiogenesis: a harmonized target for recovery after stroke. Stroke. 2012;43: 2270–2274. doi:10.1161/STROKEAHA.111.642710

99. Greenberg DA. Cerebral angiogenesis: a realistic therapy for ischemic disease? Methods Mol Biol Clifton NJ. 2014;1135: 21–24. doi:10.1007/978-1-4939-0320-7_2

100. Hatakeyama M, Ninomiya I, Kanazawa M. Angiogenesis and neuronal remodeling after ischemic stroke. Neural Regen Res. 2020;15: 16–19. doi:10.4103/1673-5374.264442

101. Bandet MV, Dong B, Winship IR. Distinct patterns of activity in individual cortical neurons and local networks in primary somatosensory cortex of mice evoked by square-wave mechanical limb stimulation. PloS One. 2021;16: e0236684. doi:10.1371/journal.pone.0236684

102. Zaletel M, Strucl M, Pretnar-Oblak J, Zvan B. Age-related changes in the relationship between visual evoked potentials and visually evoked cerebral blood flow velocity response. Funct Neurol. 2005;20: 115–120.

103. Topcuoglu MA, Aydin H, Saka E. Occipital cortex activation studied with simultaneous recordings of functional transcranial Doppler ultrasound (fTCD) and visual evoked potential (VEP) in cognitively normal human subjects: effect of healthy aging. Neurosci Lett. 2009;452: 17–22. doi:10.1016/j.neulet.2009.01.030

104. Stefanova I, Stephan T, Becker-Bense S, Dera T, Brandt T, Dieterich M. Age-related changes of blood-oxygen-level-dependent signal dynamics during optokinetic stimulation. Neurobiol Aging. 2013;34: 2277–2286. doi:10.1016/j.neurobiolaging.2013.03.031

105. Fabiani M, Gordon BA, Maclin EL, Pearson MA, Brumback-Peltz CR, Low KA, et al. Neurovascular coupling in normal aging: a combined optical, ERP and fMRI study. NeuroImage. 2014;85 Pt 1: 592–607. doi:10.1016/j.neuroimage.2013.04.113

106. Sorond FA, Hurwitz S, Salat DH, Greve DN, Fisher NDL. Neurovascular coupling, cerebral white matter integrity, and response to cocoa in older people. Neurology. 2013;81: 904–909. doi:10.1212/WNL.0b013e3182a351aa

107. Park L, Anrather J, Girouard H, Zhou P, Iadecola C. Nox2-derived reactive oxygen species mediate neurovascular dysregulation in the aging mouse brain. J Cereb Blood Flow Metab Off J Int Soc Cereb Blood Flow Metab. 2007;27: 1908–1918. doi:10.1038/sj.jcbfm.9600491

108. Menon BK, Smith EE, Coutts SB, Welsh DG, Faber JE, Goyal M, et al. Leptomeningeal collaterals are associated with modifiable metabolic risk factors. Ann Neurol. 2013;74: 241–248. doi:10.1002/ana.23906

109. Faber JE, Zhang H, Lassance-Soares RM, Prabhakar P, Najafi AH, Burnett MS, et al. Aging causes collateral rarefaction and increased severity of ischemic injury in multiple tissues. Arterioscler Thromb Vasc Biol. 2011;31: 1748–1756. doi:10.1161/ATVBAHA.111.227314

110. Strandgaard S. Cerebral blood flow in the elderly: Impact of hypertension and antihypertensive treatment. Cardiovasc Drugs Ther. 1991;4: 1217–1221. doi:10.1007/BF00114223

111. Ay H, Koroshetz WJ, Vangel M, Benner T, Melinosky C, Zhu M, et al. Conversion of ischemic brain tissue into infarction increases with age. Stroke. 2005;36: 2632–2636. doi:10.1161/01.STR.0000189991.23918.01

112. Bullmore E, Sporns O. Complex brain networks: graph theoretical analysis of structural and functional systems. Nat Rev Neurosci. 2009;10: 186–198. doi:10.1038/nrn2575

113. Sporns O. The non-random brain: efficiency, economy, and complex dynamics. Front Comput Neurosci. 2011;5: 5. doi:10.3389/fncom.2011.00005

114. Stam CJ. Modern network science of neurological disorders. Nat Rev Neurosci. 2014;15: 683–695. doi:10.1038/nrn3801

115. Berkes P, Orbán G, Lengyel M, Fiser J. Spontaneous cortical activity reveals hallmarks of an optimal internal model of the environment. Science. 2011;331: 83–87. doi:10.1126/science.1195870

116. Cossart R, Aronov D, Yuste R. Attractor dynamics of network UP states in the neocortex. Nature. 2003;423: 283–288. doi:10.1038/nature01614

117. Harris KD, Csicsvari J, Hirase H, Dragoi G, Buzsáki G. Organization of cell assemblies in the hippocampus. Nature. 2003;424: 552–556. doi:10.1038/nature01834

118. Hyman JM, Whitman J, Emberly E, Woodward TS, Seamans JK. Action and outcome activity state patterns in the anterior cingulate cortex. Cereb Cortex N Y N 1991. 2013;23: 1257–1268. doi:10.1093/cercor/bhs104

119. Malvache A, Reichinnek S, Villette V, Haimerl C, Cossart R. Awake hippocampal reactivations project onto orthogonal neuronal assemblies. Science. 2016;353: 1280–1283. doi:10.1126/science.aaf3319

120. Miller JK, Ayzenshtat I, Carrillo-Reid L, Yuste R. Visual stimuli recruit intrinsically generated cortical ensembles. Proc Natl Acad Sci U S A. 2014;111: E4053-4061. doi:10.1073/pnas.1406077111

121. Sakata S, Harris KD. Laminar structure of spontaneous and sensory-evoked population activity in auditory cortex. Neuron. 2009;64: 404–418. doi:10.1016/j.neuron.2009.09.020

122. See JZ, Atencio CA, Sohal VS, Schreiner CE. Coordinated neuronal ensembles in primary auditory cortical columns. eLife. 7: e35587. doi:10.7554/eLife.35587

123. Truccolo W, Hochberg LR, Donoghue JP. Collective dynamics in human and monkey sensorimotor cortex: predicting single neuron spikes. Nat Neurosci. 2010;13: 105–111. doi:10.1038/nn.2455

124. Villette V, Malvache A, Tressard T, Dupuy N, Cossart R. Internally Recurring Hippocampal Sequences as a Population Template of Spatiotemporal Information. Neuron. 2015;88: 357–366. doi:10.1016/j.neuron.2015.09.052

125. Avitan L, Pujic Z, Mölter J, Van De Poll M, Sun B, Teng H, et al. Spontaneous Activity in the Zebrafish Tectum Reorganizes over Development and Is Influenced by Visual Experience. Curr Biol CB. 2017;27: 2407-2419.e4. doi:10.1016/j.cub.2017.06.056

126. Pietri T, Romano SA, Pérez-Schuster V, Boulanger-Weill J, Candat V, Sumbre G. The Emergence of the Spatial Structure of Tectal Spontaneous Activity Is Independent of Visual Inputs. Cell Rep. 2017;19: 939–948. doi:10.1016/j.celrep.2017.04.015

127. Thompson AW, Scott EK. Characterisation of sensitivity and orientation tuning for visually responsive ensembles in the zebrafish tectum. Sci Rep. 2016;6: 34887. doi:10.1038/srep34887

128. Luczak A, Barthó P, Harris KD. Spontaneous events outline the realm of possible sensory responses in neocortical populations. Neuron. 2009;62: 413–425. doi:10.1016/j.neuron.2009.03.014

129. MacLean JN, Watson BO, Aaron GB, Yuste R. Internal dynamics determine the cortical response to thalamic stimulation. Neuron. 2005;48: 811–823. doi:10.1016/j.neuron.2005.09.035

130. Carey LM, Matyas TA. Frequency of discriminative sensory loss in the hand after stroke in a rehabilitation setting. J Rehabil Med. 2011;43: 257–263. doi:10.2340/16501977-0662

131. Connell LA, Lincoln NB, Radford KA. Somatosensory impairment after stroke: frequency of different deficits and their recovery. Clin Rehabil. 2008;22: 758–767. doi:10.1177/0269215508090674

132. Kwakkel G, Kollen B, Lindeman E. Understanding the pattern of functional recovery after stroke: facts and theories. Restor Neurol Neurosci. 2004;22: 281–299.

133. Patel AT, Duncan PW, Lai SM, Studenski S. The relation between impairments and functional outcomes poststroke. Arch Phys Med Rehabil. 2000;81: 1357–1363. doi:10.1053/apmr.2000.9397

134. Tyson SF, Hanley M, Chillala J, Selley AB, Tallis RC. Sensory loss in hospital-admitted people with stroke: characteristics, associated factors, and relationship with function. Neurorehabil Neural Repair. 2008;22: 166–172. doi:10.1177/1545968307305523

135. Brecht M, Schneider M, Sakmann B, Margrie TW. Whisker movements evoked by stimulation of single pyramidal cells in rat motor cortex. Nature. 2004;427: 704–710. doi:10.1038/nature02266

136. Houweling AR, Brecht M. Behavioural report of single neuron stimulation in somatosensory cortex. Nature. 2008;451: 65–68. doi:10.1038/nature06447

137. Simoncelli EP, Olshausen BA. Natural image statistics and neural representation. Annu Rev Neurosci. 2001;24: 1193–1216. doi:10.1146/annurev.neuro.24.1.1193

138. Barlow H. Redundancy reduction revisited. Netw Bristol Engl. 2001;12: 241–253.

139. Holtmaat A, Bonhoeffer T, Chow DK, Chuckowree J, De Paola V, Hofer SB, et al. Long-term, high-resolution imaging in the mouse neocortex through a chronic cranial window. Nat Protoc. 2009;4: 1128–1144. doi:10.1038/nprot.2009.89

140. Blackwell AA, Banovetz MT, Qandeel, Whishaw IQ, Wallace DG. The structure of arm and hand movements in a spontaneous and food rewarded on-line string-pulling task by the mouse. Behav Brain Res. 2018;345: 49–58. doi:10.1016/j.bbr.2018.02.025

141. Inayat S, Singh S, Ghasroddashti A, Qandeel, Egodage P, Whishaw IQ, et al. A Matlab-based toolbox for characterizing behavior of rodents engaged in string-pulling. Kleinfeld D, Wassum KM, editors. eLife. 2020;9: e54540. doi:10.7554/eLife.54540

142. Blackwell AA, Köppen JR, Whishaw IQ, Wallace DG. String-pulling for food by the rat:

Assessment of movement, topography and kinematics of a bilaterally skilled forelimb act. Learn Motiv. 2018;61: 63–73. doi:10.1016/j.lmot.2017.03.010

143. Kislin M, Mugantseva E, Molotkov D, Kulesskaya N, Khirug S, Kirilkin I, et al. Flat-floored Air-lifted Platform: A New Method for Combining Behavior with Microscopy or Electrophysiology on Awake Freely Moving Rodents. JoVE J Vis Exp. 2014; e51869. doi:10.3791/51869

144. Schindelin J, Arganda-Carreras I, Frise E, Kaynig V, Longair M, Pietzsch T, et al. Fiji: an open-source platform for biological-image analysis. Nat Methods. 2012;9: 676–682. doi:10.1038/nmeth.2019

145. Peron S, Chen T-W, Svoboda K. Comprehensive imaging of cortical networks. Curr Opin Neurobiol. 2015;32: 115–123. doi:10.1016/j.conb.2015.03.016

146. Hendrickson AE, White PO. Promax: A Quick Method for Rotation to Oblique Simple Structure. Br J Stat Psychol. 1964;17: 65–70. doi:10.1111/j.2044-8317.1964.tb00244.x

147. Hilgetag CC, Kötter R, Stephan KE, Sporns O. Computational Methods for the Analysis of Brain Connectivity. In: Ascoli GA, editor. Computational Neuroanatomy: Principles and Methods. Totowa, NJ: Humana Press; 2002. pp. 295–335. doi:10.1007/978-1-59259-275-3_14

148. Sporns O, Honey CJ, Kötter R. Identification and Classification of Hubs in Brain Networks. PLOS ONE. 2007;2: e1049. doi:10.1371/journal.pone.0001049

149. Chen T-W, Wardill TJ, Sun Y, Pulver SR, Renninger SL, Baohan A, et al. Ultra-sensitive fluorescent proteins for imaging neuronal activity. Nature. 2013;499: 295–300. doi:10.1038/nature12354

150. Dana H, Sun Y, Mohar B, Hulse BK, Kerlin AM, Hasseman JP, et al. High-performance calcium sensors for imaging activity in neuronal populations and microcompartments. Nat Methods. 2019;16: 649–657. doi:10.1038/s41592-019-0435-6

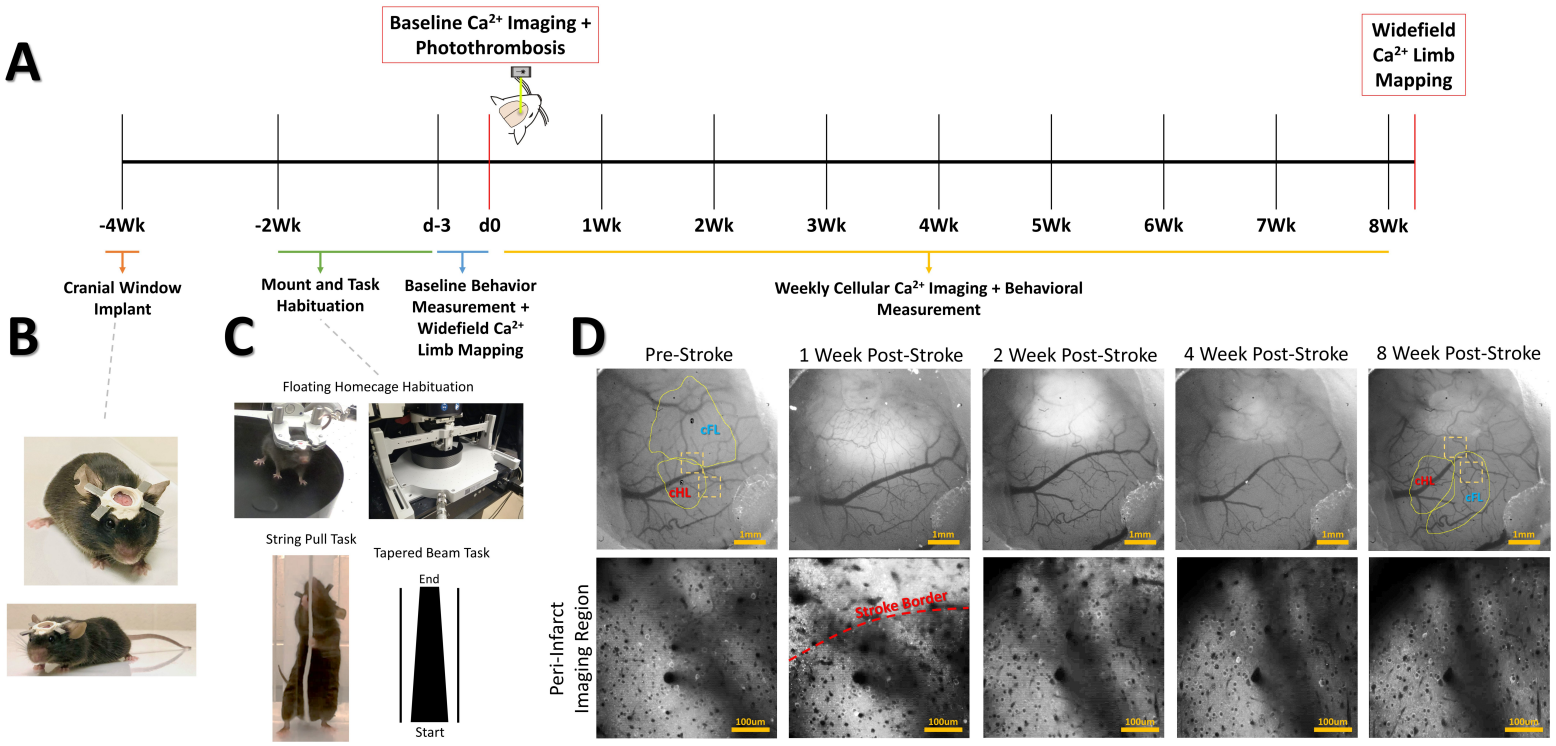
A
Baseline Ca2+ Imaging + Photothrombosis
Widefield Ca2+ Limb Mapping
-4Wk
-2Wk
d-3
d0
1Wk
2Wk
3Wk
4Wk
5Wk
6Wk
7Wk
8Wk
Cranial Window Implant
Mount and Task Habituation
Baseline Behavior Measurement + Widefield Ca2+ Limb Mapping
Weekly Cellular Ca2+ Imaging + Behavioral Measurement
B
C
Floating Homecage Habituation
String Pull Task
Tapered Beam Task
End
Start
D
Pre-Stroke
1 Week Post-Stroke
2 Week Post-Stroke
4 Week Post-Stroke
8 Week Post-Stroke
cFL
cHL
1mm
Peri-Infarct Imaging Region
Stroke Border
100um

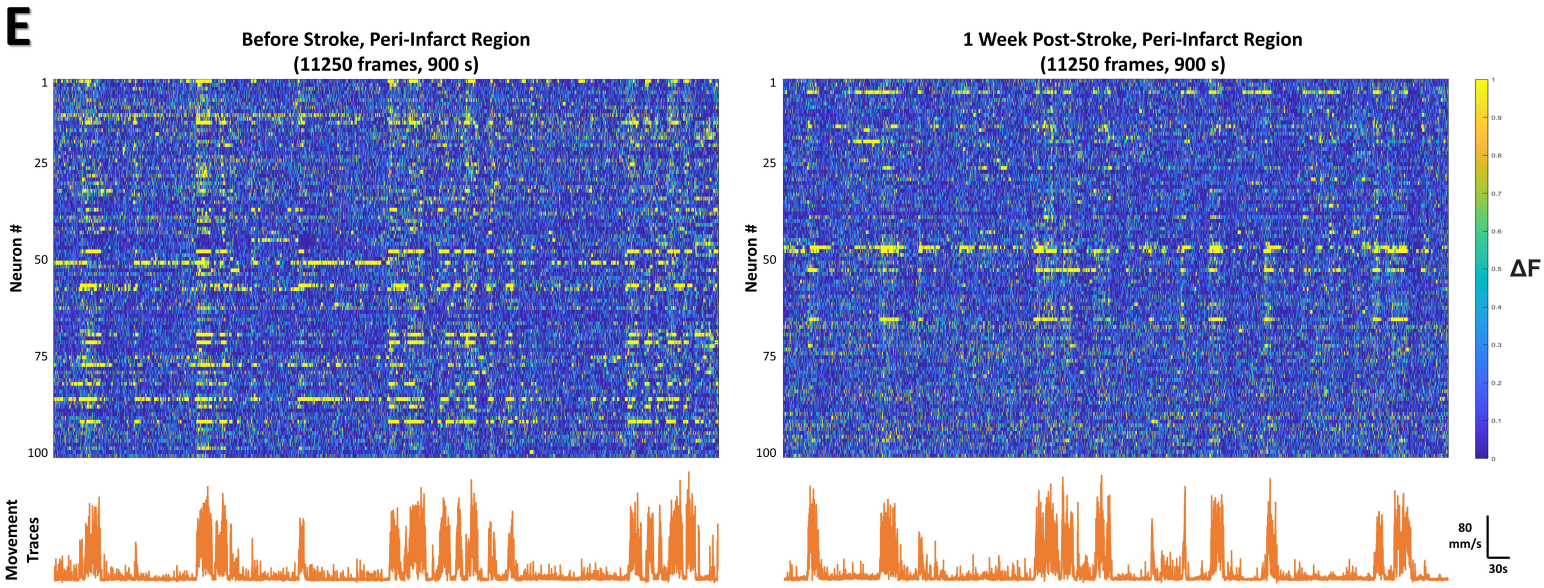
E
Before Stroke, Peri-Infarct Region (11250 frames, 900 s)
1 Week Post-Stroke, Peri-Infarct Region (11250 frames, 900 s)
Neuron #
1
25
50
75
100
ΔF
Movement Traces
80 mm/s
30s

Fig 1. Experimental timeline and methods. (**A**) Timeline of experimental procedures, imaging times, and behavioral tests. (**B**) Glass cranial windows and headplates were implanted 2-weeks prior to beginning habituation protocols in Thy1-GCaMP6S mice. (**C**) Mice were habituated on the floating homecage, string pull and tapered beam for a period of 2-weeks prior to baseline measurements for behavior. Widefield Ca2+ response maps were used to determine locations for the imaging site located between the cFL and cHL sensory maps at baseline ("peri-infarct" imaging region) and imaging site lateral to the cHL at baseline ("distal" imaging region). For each Ca^{2+} imaging session, both imaging regions were imaged for a period of 15 minutes while simultaneously tracking animal movement within the mobile homecage. After baseline Ca^{2+} imaging, the somatosensory cFL map was targeted with photothrombosis. Behavioral testing on the string pull task and tapered beam task were performed weekly 1 day prior to the Ca^{2+} imaging session. After the final cellular Ca^{2+} imaging session at the 8-week time, stimulus-evoked widefield Ca^{2+} imaging was once again performed to determine the cFL and cHL somatosensory maps. (**D**) Representative widefield and two photon calcium imaging at each weekly time. The area of decreased light absorption due to stroke damage is apparent, with its surface area decreasing over time. (**E**) Neuron Ca^{2+} traces ($\Delta F/F_o$) for 100 neurons from one example animal pre-stroke (left panel) and 1-week post-stroke (right panel) in the peri-infarct somatosensory imaging region. Lower line graphs demonstrate the tracked movement (mm/s) within the floating homecage corresponding to the Ca^{2+} traces above.

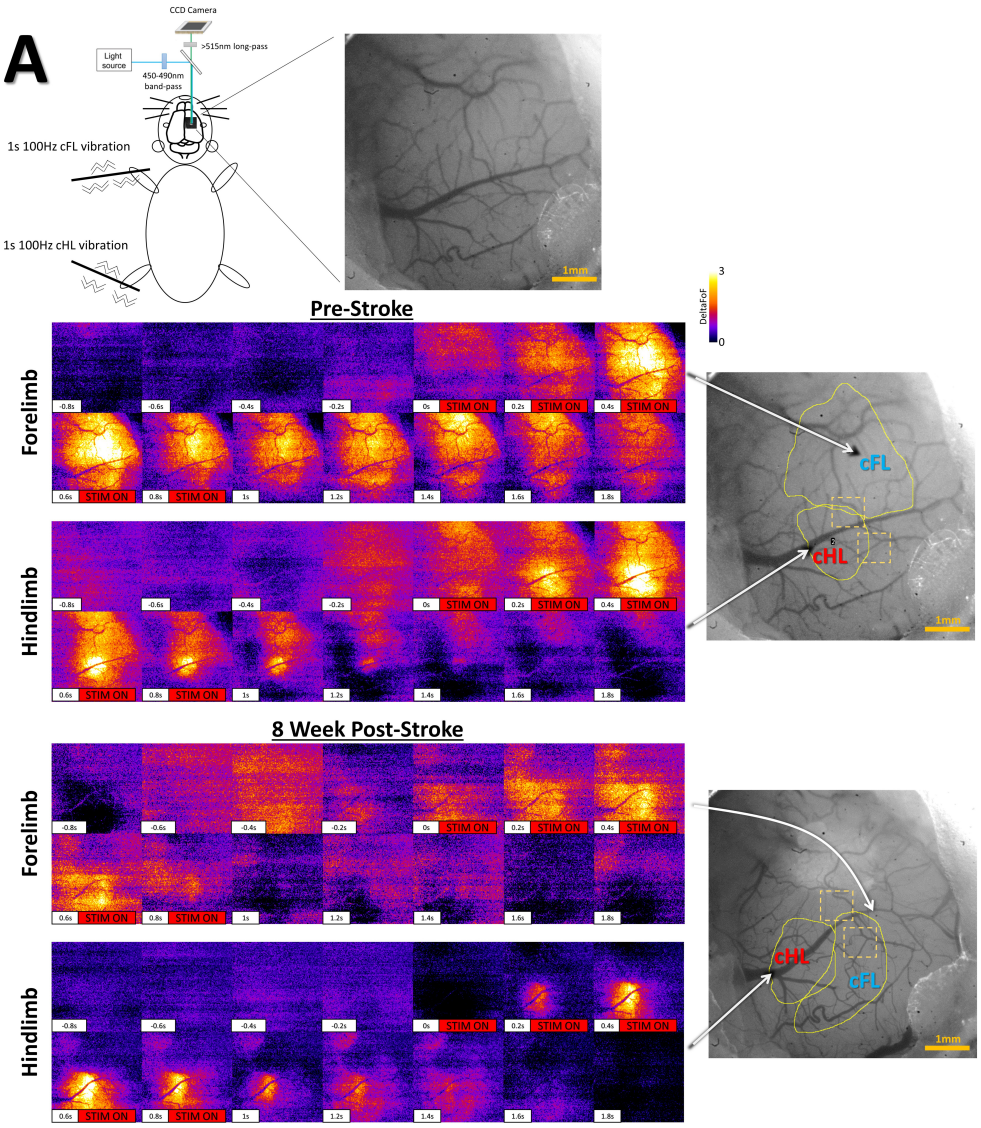
A
CCD Camera
>515nm long-pass
Light source
450-490nm band-pass
1s 100Hz cFL vibration
1s 100Hz cHL vibration
1mm
Pre-Stroke
Forelimb
Hindlimb
DeltaFoF
3
0
-0.8s
-0.6s
-0.4s
-0.2s
0s
STIM ON
0.2s
0.4s
0.6s
0.8s
1s
1.2s
1.4s
1.6s
1.8s
cFL
cHL
8 Week Post-Stroke

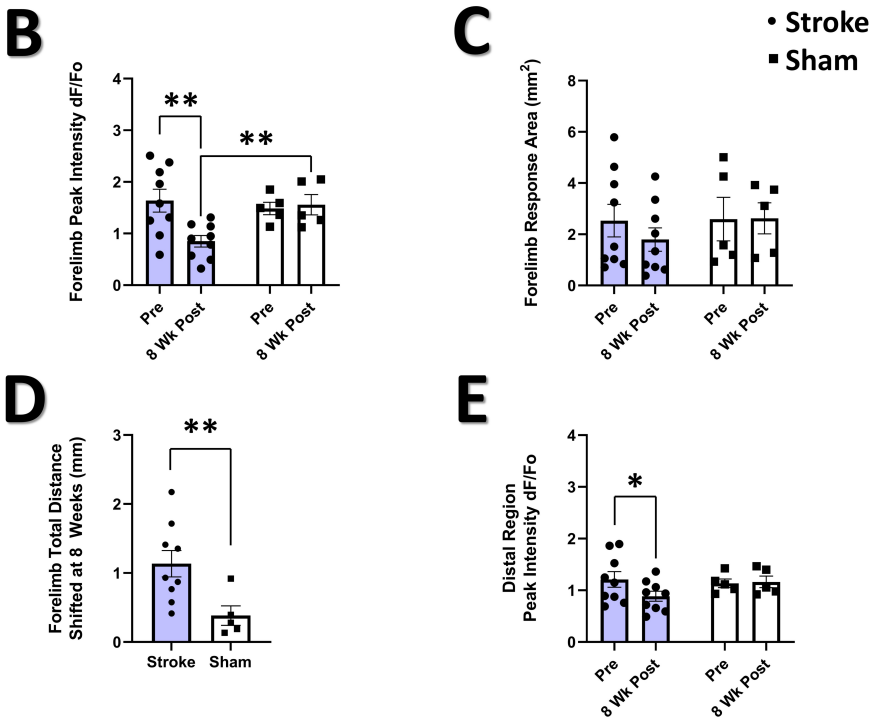
B
Forelimb Peak Intensity dF/Fo
**
**
Pre
8 Wk Post
Pre
8 Wk Post
C
• Stroke
▪ Sham
Forelimb Response Area (mm²)
Pre
8 Wk Post
Pre
8 Wk Post
D
Forelimb Total Distance Shifted at 8 Weeks (mm)
**
Stroke
Sham
E
Distal Region Peak Intensity dF/Fo
*
Pre
8 Wk Post
Pre
8 Wk Post

Fig 2. Photothrombotic stroke results in forelimb representation shift onto adjacent areas of cortex and altered sensory-evoked widefield Ca^{2+} response properties at 8-weeks post-stroke. (**A**) Pseudocolored ($\Delta F/F_o$) montages of representative cFL and cHL responses in S1 of an anesthetized animal pre-stroke and 8-week post-stroke resulting from oscillatory stimulation (1s, 100 Hz) of the cFL and cHL, respectively. At the 8-week post-stroke time, the cFL map has shifted posterior to its pre-stroke location into the area lateral to the cHL. (**B**) Mean peak forelimb Ca^{2+} transient response intensity ($\Delta F/F_o$) measured from the thresholded cortical map area of the cFL. A significant interaction between group and time was found, with *post-hoc* tests showing a significant decrease in the peak cFL response at 8-week post-stroke compared to pre-stroke ($P = 0.0055$) and compared to 8-week sham ($P = 0.0277$). Mixed Effects Model, Time $F_{(1, 12)} = 4.151$, $P = 0.0643$; Group $F_{(1, 12)} = 1.909$, $P = 0.1922$; Interaction $F_{(1, 12)} = 6.010$, $P = 0.0305$. (**C**) Thresholded cFL response area (mm^2). No main effects or interaction was observed. (**D**) The stroke group was found to have significantly greater total distance shifted for the forelimb map at the 8-week time compared to sham ($P = 0.0080$). (**E**) Mean peak forelimb Ca^{2+} transient response intensity ($\Delta F/F_o$) measured from the distal region ROI lateral to the hindlimb response map. *Post-hoc* tests show a decrease in distal region peak response intensity at 8-weeks in the stroke group ($P=0.0442$). Mixed Effects Model, Time $F_{(1, 12)} = 2.054$, $P = 0.1773$; Group $F_{(1, 12)} = 0.4256$, $P = 0.5264$; Interaction $F_{(1, 12)} = 2.889$, $P = 0.1150$. Stroke N = 9, Sham N = 5. *$p < 0.05$; **$p < 0.01$; ***$p < 0.001$

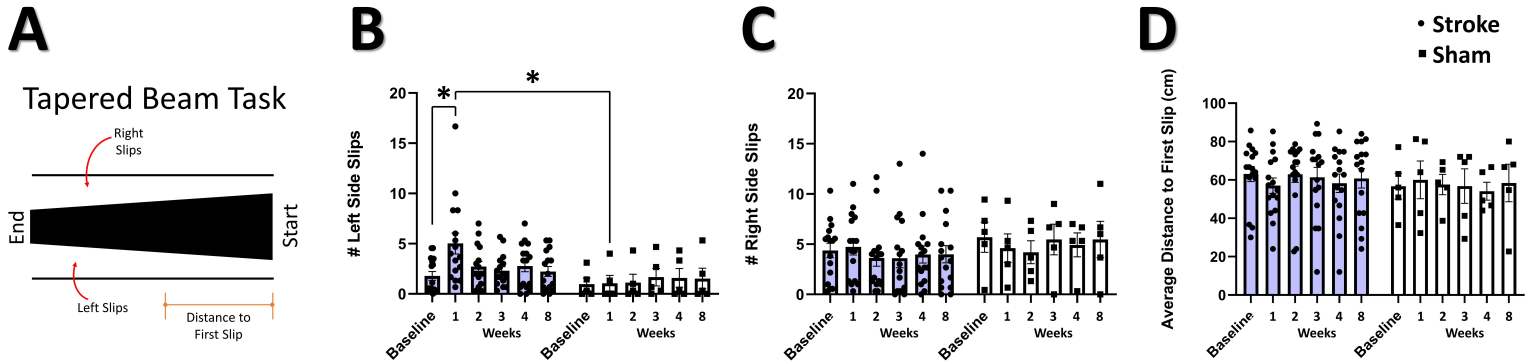
A
Tapered Beam Task
Right Slips
End
Start
Left Slips
Distance to First Slip
B
Left Side Slips
Baseline
Weeks
C
Right Side Slips
D
Stroke
Sham
Average Distance to First Slip (cm)

Fig 3. Impaired performance on tapered beam task after stroke. (**A**) Illustration of the tapered beam test with the three elements measured; left (contralesional) side slips, right side slips, and distance to first slip. (**B**) Mean number of left side slips. A significant interaction between time and group was observed, with *post-hoc* tests showing a greater number of left side slips at 1-week in the stroke group relative to the sham group ($P = 0.0435$), and in the stroke group at 1-week relative to baseline ($P = 0.0125$). Mixed Effects Model, Time $F_{(2.007, 38.13)} = 2.178$, $P = 0.1270$; Group $F_{(1, 19)} = 2.260$; $P = 0.1492$; Interaction $F_{(5, 95)} = 2.914$, $P = 0.0172$. (**C**) Mean number of right-side slips. No main effects or interactions were observed. (**D**) Distance to first slip. No main effects or interactions were observed. Stroke N = 16, Sham N = 5. *$p < 0.05$; **$p < 0.01$; ***$p < 0.001$

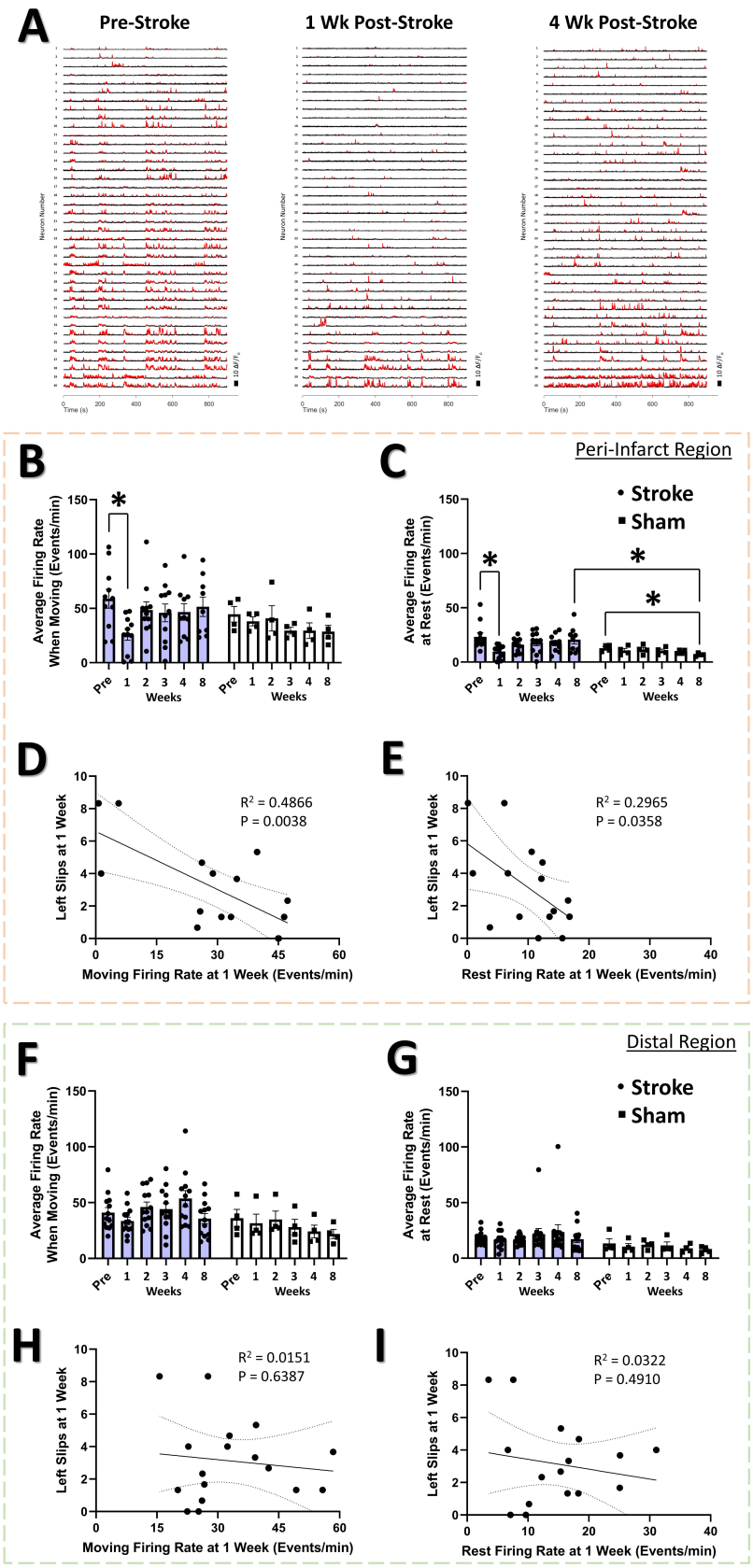
A
Pre-Stroke
1 Wk Post-Stroke
4 Wk Post-Stroke
B
Average Firing Rate When Moving (Events/min)
Weeks
C
Peri-Infarct Region
• Stroke
▪ Sham
Average Firing Rate at Rest (Events/min)
D
Left Slips at 1 Week
R² = 0.4866
P = 0.0038
Moving Firing Rate at 1 Week (Events/min)
E
R² = 0.2965
P = 0.0358
Rest Firing Rate at 1 Week (Events/min)
F
G
Distal Region
H
R² = 0.0151
P = 0.6387
I
R² = 0.0322
P = 0.4910

Fig 4. Firing rate of neurons in the peri-infarct cortex correlates with performance on the tapered beam task. (**A**) Example Ca^{2+} traces for 40 example neurons at each time point from the peri-infarct imaging region for one example animal in the stroke group. Significant Ca^{2+} transients are highlighted by red segments. A decrease in the number of Ca^{2+} transients is visually apparent at 1-week post-stroke. (**B**) In the peri-infarct imaging region, no main effects or interaction was seen in the average firing rate during animal movement, however *post-hoc* analysis indicates significantly decreased average firing rate at 1-week in the stroke group relative to pre-stroke (P = 0.0124). Mixed Effects Model, Time $F_{(3.217, 39.89)} = 1.629$, P = 0.1953; Group $F_{(1, 13)} = 1.106$, P = 0.3121; Interaction $F_{(5, 62)} = 1.079$, P = 0.3810. A significant main effect of group was seen in the average firing rate at rest (**C**), with *post-hoc* tests showing a significant decrease a 1-week post-stroke compared to pre-stroke (P = 0.0325), a significant decrease at 8-weeks post-sham compared with pre-sham (P = 0.0280), and significantly lower at 8-weeks post-sham compared with 8-weeks post-stroke (P = 0.0439). Mixed Effects Model, Time $F_{(2.297, 28.48)} = 1.360$, P = 0.2742; Group $F_{(1, 13)} = 6.058$, P = 0.0286; Interaction $F_{(5, 62)} = 1.169$, P = 0.3346). Average firing rate 1-week post-stroke was negatively correlated with the number of left slips in the tapered beam at the same 1-week time during both movement ($R^2 = 0.4866$, P = 0.0038) (**D**) and rest ($R^2 = 0.2965$, P = 0.0358) (**E**). In the distal imaging region, no main effects or interaction were found in the average firing rate for movement (**F)** or at rest (**G**). No correlation was observed between the moving firing rate at 1-week in the distal region and the number of left slips on the tapered beam ($R^2 = 0.0151$, P = 0.6387) (**H**). No correlation was observed between the resting firing rate at 1-week in the distal region and the number of left slips on the tapered beam ($R^2 = 0.0322$, P = 0.4910) (**I**). Peri-infarct region Stroke N = 11, Sham N = 4. Distal region Stroke N = 13, Sham N = 4. *p < 0.05; **p < 0.01; ***p < 0.001

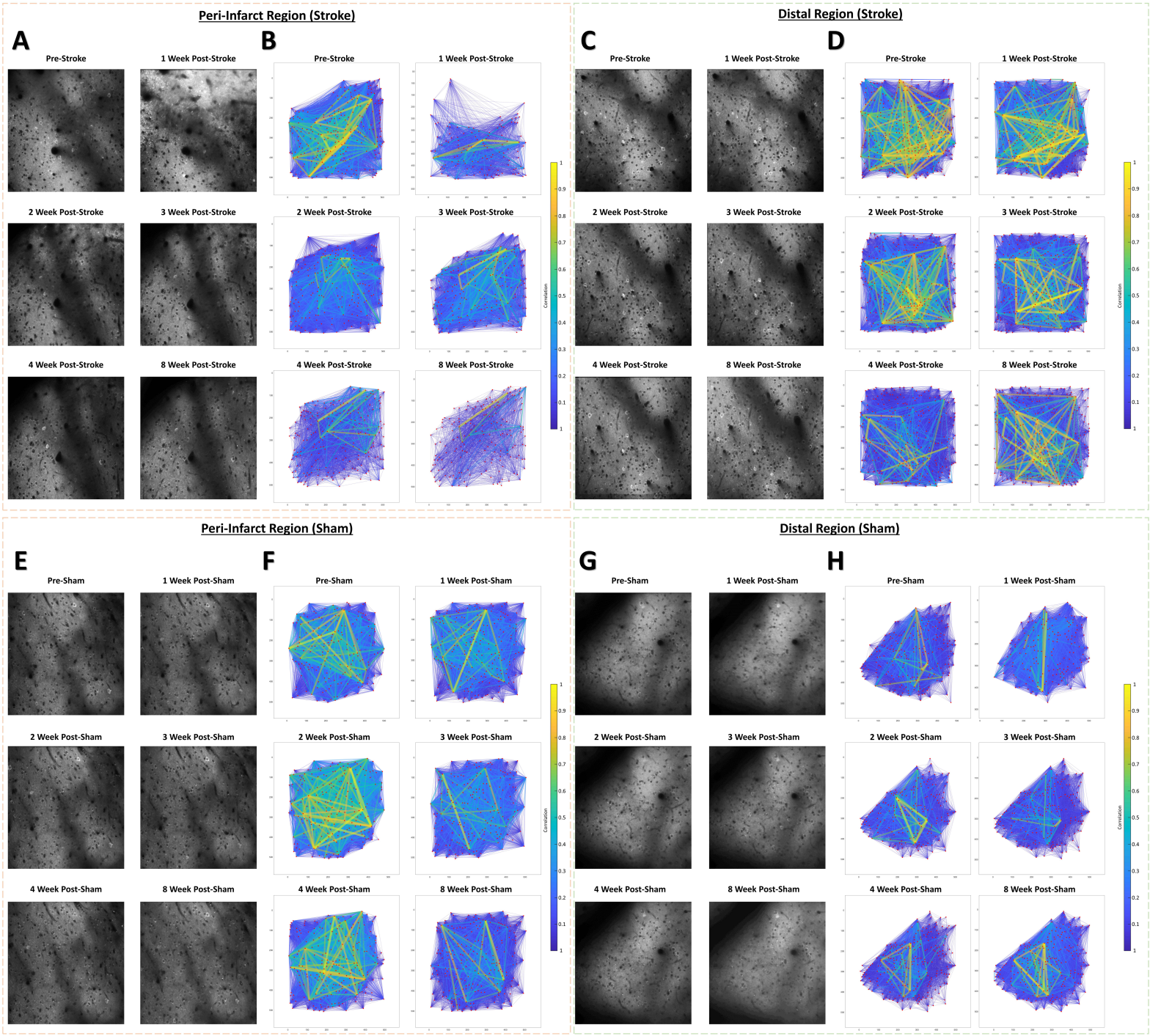
Peri-Infarct Region (Stroke)
Distal Region (Stroke)
Peri-Infarct Region (Sham)
Distal Region (Sham)
A
B
C
D
E
F
G
H
Pre-Stroke
1 Week Post-Stroke
2 Week Post-Stroke
3 Week Post-Stroke
4 Week Post-Stroke
8 Week Post-Stroke
Pre-Sham
1 Week Post-Sham
2 Week Post-Sham
3 Week Post-Sham
4 Week Post-Sham
8 Week Post-Sham
Correlation

Fig 5. Example cellular GCaMP6S Ca^{2+} fluorescence images and population functional connectivity plots. (**A-D**) Ca^{2+} fluorescence images and functional connectivity plots from the peri-infarct imaging region and the distal imaging region for one example stroke group animal. Population functional connectivity plots demonstrate neurons as red dots, and the functional connection strength as lines with color and line width determined by the strength of the correlation between neurons. Notable cortical damage is visible in the upper portion of the 1-week post-stroke Ca^{2+} fluorescence image in the peri-infarct imaging region (**A**), which notably improves over the 2-4 week times. A notable loss of functional connections and loss in the number of connections with strong correlation (>0.3) is visible in the functional connectivity plots at 1-week post-stroke in the peri-infarct imaging region (**B**). In the distal imaging region post-stroke, little structural change is visible in the cellular Ca^{2+} fluorescence images (**C**), and less change to functional connectivity of the population over time (**D**). (**E-H**) Ca^{2+} fluorescence images and functional connectivity plots from the peri-infarct imaging region and the distal imaging region for one example sham group animal. Little structural changes within the cellular Ca^{2+} fluorescence images and in the functional connectivity plots are visually apparent relative to the example stroke animal.

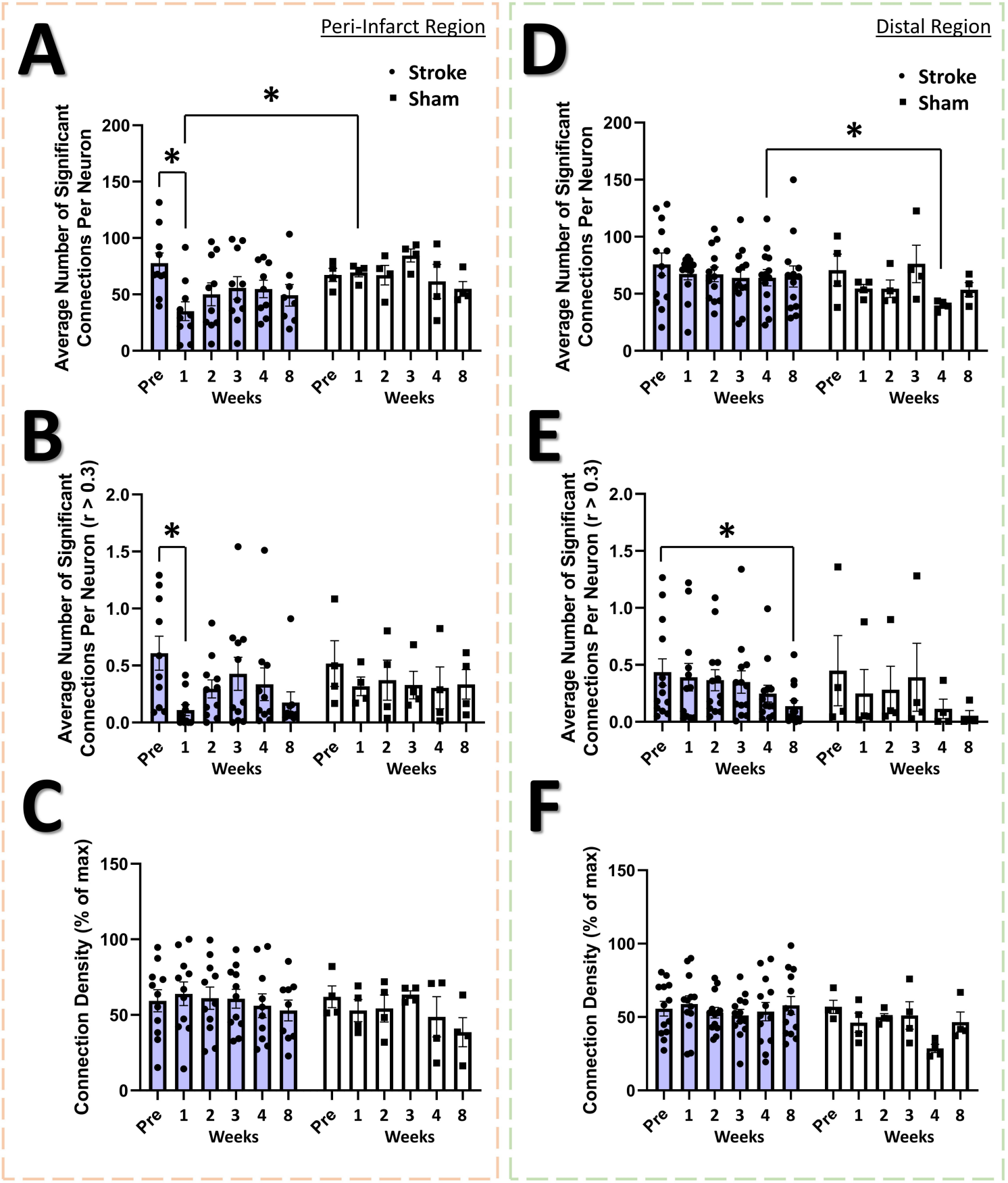
A
Peri-Infarct Region
Stroke
Sham
Average Number of Significant Connections Per Neuron
Pre 1 2 3 4 8 Pre 1 2 3 4 8
Weeks
B
Average Number of Significant Connections Per Neuron (r > 0.3)
C
Connection Density (% of max)
D
Distal Region
E
F

Fig 6. Altered functional connectivity in the peri-infarct somatosensory cortex. In the peri-infarct imaging region, a trend of a main effect of time was found in the average number of significant connections per neuron (**A**), with *post-hoc* tests showing a significant decrease at 1-week post-stroke relative to pre-stroke (P = 0.0373) and relative to 1-week post-sham (P = 0.0178). Mixed Effects Model, Time $F_{(3.559, 40.58)} = 2.213$, P = 0.0914 ; Group $F_{(1, 12)} = 1.716$, P = 0.2147; Interaction $F_{(5, 57)} = 1.820$, P = 0.1233. A significant main effect of time was found in the average number of significant connections per neurons with correlation greater than 0.3 (**B**), with *post-hoc* tests indicating a significant decrease at 1-week post-stroke compared to pre-stroke (P = 0.0398). Mixed Effects Model, Time $F_{(3.463, 41.55)} = 2.735$, P = 0.0484; Group $F_{(1, 13)} = 0.0964$, P = 0.7610; Interaction $F_{(5, 60)} = 0.8633$, P = 0.5111. No significant main effects or interaction is seen in the connection density for the peri-infarct imaging region (**C**). In the distal imaging region, no significant main effects or interaction is seen in the average number of significant connections per neuron (**D**), however *post-hoc* tests indicate significantly lower connections per neuron at 4-weeks in the sham group relative to 4-weeks post-stroke (P = 0.0360). Mixed Effects Model, Time $F_{(2.991, 44.87)} = 1.314$, P = 0.2815; Group $F_{(1, 15)} = 1.138$, P = 0.3030; Interaction $F_{(5, 75)} = 0.8022$, P = 0.5516. A significant main effect of time was observed for the average number of significant connections with correlation greater than 0.3 in the distal region (**E**), with *post-hoc* tests indicating a significant decrease at 8-weeks post-stroke relative to pre-stroke (P = 0.0189) Mixed Effects Model, Time $F_{(2.909, 43.06)} = 4.451$, P = 0.0088; Group $F_{(1, 15)} = 0.1272$, P = 0.7263; Interaction $F_{(5, 74)} = 0.8692$, P = 0.3676. No significant main effects or interaction is seen in the connection density (**F**). Peri-infarct region Stroke N = 11, Sham N = 4. Distal region Stroke N = 13, Sham N = 4. *p < 0.05; **p < 0.01; ***p < 0.001

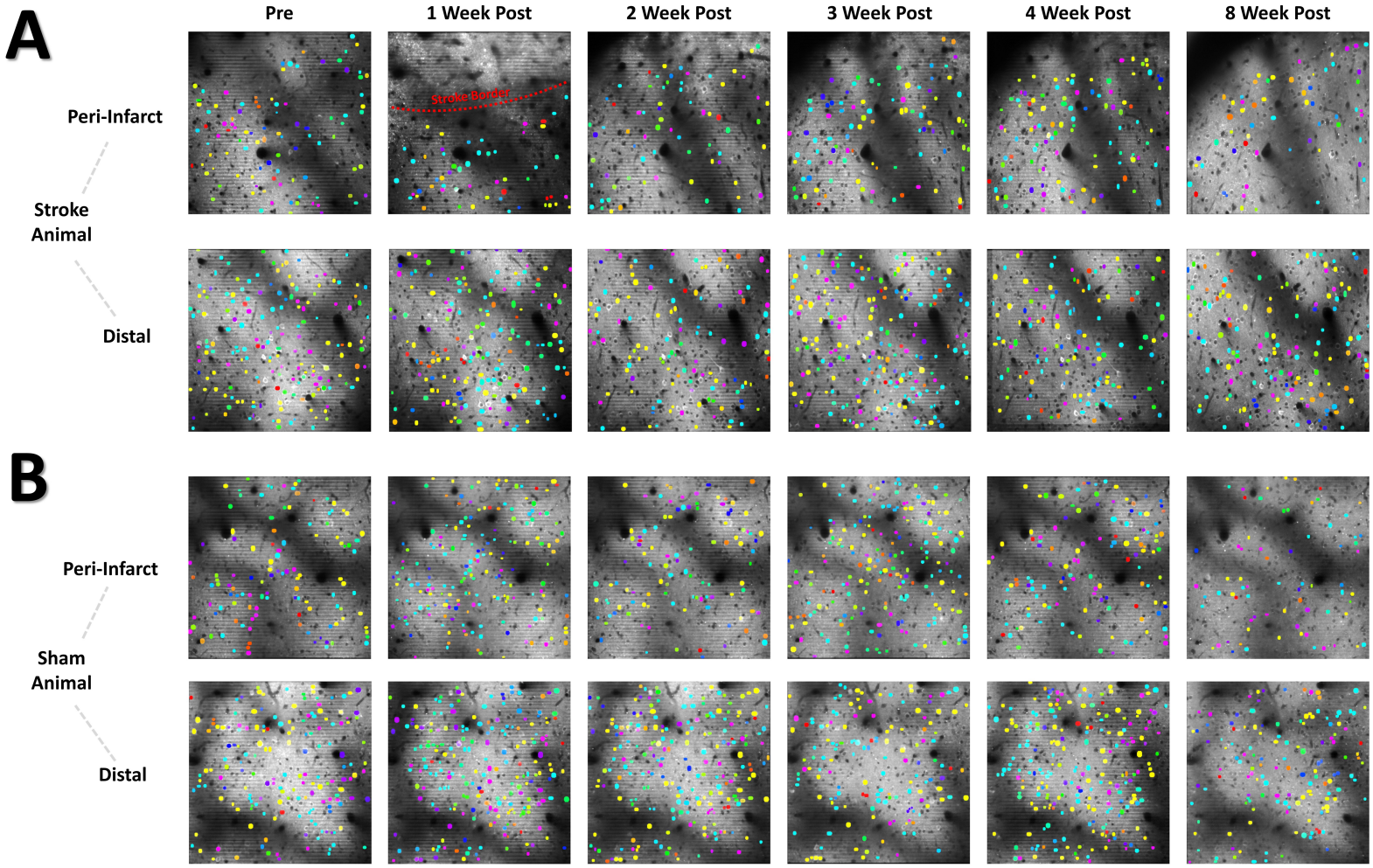
A
Pre
1 Week Post
2 Week Post
3 Week Post
4 Week Post
8 Week Post
Peri-Infarct
Stroke Animal
Distal
Stroke Border
B
Peri-Infarct
Sham Animal
Distal

Fig 7. Color coded neural assembly plots depict altered neural assembly architecture after stroke in the peri-infarct region. (**A**) Representative cellular Ca^{2+} fluorescence images with neural assemblies color coded and overlaid for each timepoint. Neurons belonging to the same assembly have been pseudocolored with identical color. A loss in the number of neural assemblies after stroke in the peri-infarct region is visually apparent, along with a concurrent increase in the number of neurons for each remaining assembly. (**B**) Representative sham animal displays no visible change in the number of assemblies or number of neurons per assembly.

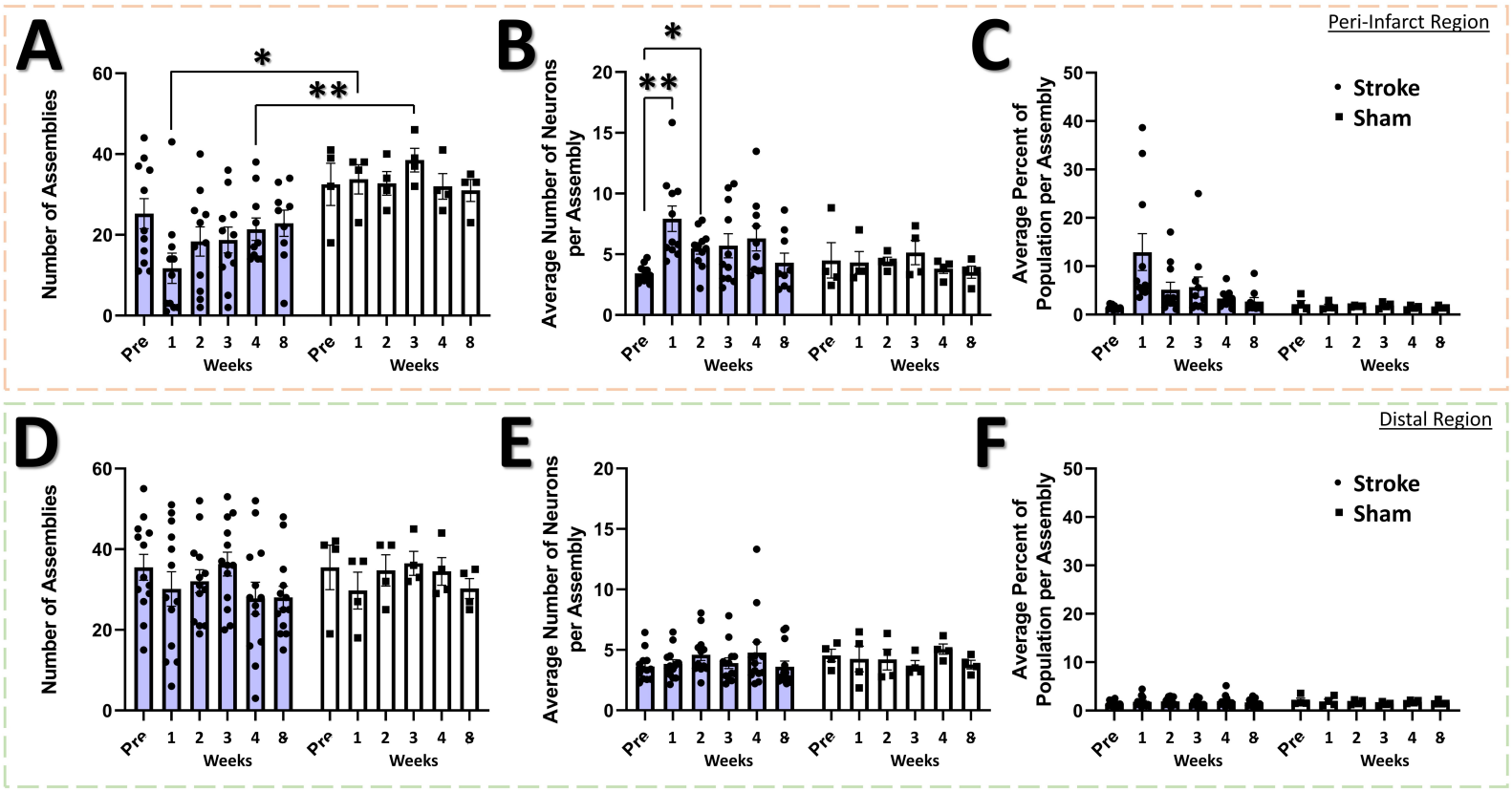
A
B
C
Peri-Infarct Region
Number of Assemblies
Average Number of Neurons per Assembly
Average Percent of Population per Assembly
Stroke
Sham
Weeks
Pre
1
2
3
4
8
D
E
F
Distal Region

Fig 8. Neural assembly structure is disrupted in the peri-infarct region after stroke. In the peri-infarct imaging region, a significant main effect of group was found for the number of assemblies (**A**), with *post-hoc* tests showing a significant decrease in the number of assemblies at the 1-week and 3-week times for the stroke group compared to sham (P = 0.0114 & 0.0058, respectively). Mixed Effects Model, Time $F_{(2.883, 35.75)} = 0.8231$, P = 0.4857; Group $F_{(1, 13)} = 11.90$, P = 0.0043; Interaction $F_{(5, 62)} = 1.496$, P = 0.2040. No main effects or interaction was observed in the average number of neurons per assembly (**B)**, however *post-hoc* tests indicated significantly higher number of neurons at 1- and 2-weeks post-stroke compared to pre-stroke (P = 0.0099 and 0.0190, respectively). Mixed Effects Model, Time $F_{(3.405, 42.22)} = 1.865$, P = 0.1435; Group $F_{(1, 13)} = 2.018$, P = 0.1790; Interaction $F_{(5, 62)} = 1.728$, P = 0.1415. A trend of a main effect of group was found in the average percent of the population per assembly (**C)**, with *post-hoc* tests showing a trend at 1-week post-stroke compared to pre-stroke (P = 0.0683) and compared to 1-week post-sham (P = 0.0863). Mixed Effects Model, Time $F_{(1.711, 21.22)} = 1.738$, P = 0.2023; Group $F_{(1, 13)} = 3.807$, P = 0.0729; Interaction $F_{(5, 62)} = 1.765$, P = 0.1333. No main effects or interaction was observed in the distal imaging region for number of assemblies (**D**), average number of neurons per assembly (**E**), or average percent of the population per assembly (**F**). Peri-infarct region Stroke N = 11, Sham N = 4. Distal region Stroke N = 13, Sham N = 4. *p < 0.05; **p < 0.01; ***p < 0.001

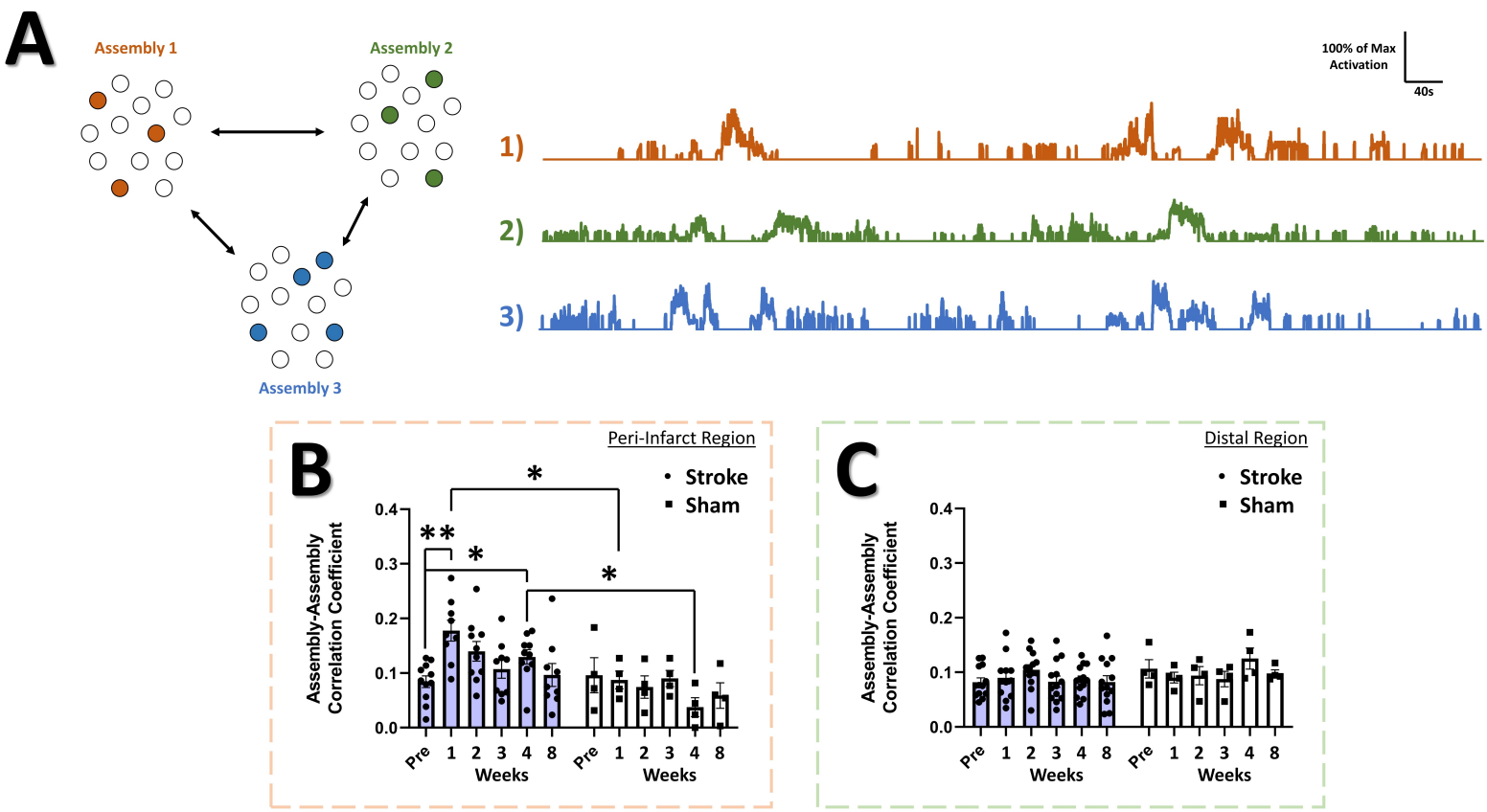
A
Assembly 1
Assembly 2
Assembly 3
100% of Max Activation
40s
1)
2)
3)
B
Peri-Infarct Region
Stroke
Sham
Assembly-Assembly Correlation Coefficient
0.4
0.3
0.2
0.1
0.0
**
*
*
*
Pre 1 2 3 4 8 Pre 1 2 3 4 8
Weeks
Weeks
C
Distal Region
Stroke
Sham
Assembly-Assembly Correlation Coefficient
0.4
0.3
0.2
0.1
0.0
Pre 1 2 3 4 8 Pre 1 2 3 4 8
Weeks
Weeks

Fig 9. Correlation among neural assemblies is increased in the peri-infarct imaging region after stroke. (**A**) Illustration of three example color coded neural assemblies from a neural population and their corresponding time series activations that were correlated. In the peri-infarct imaging region, a significant main effect of group was found in the correlation coefficient for significantly correlated assembly-assembly pairs (**B)**, with *post-hoc* tests indicating a significantly higher correlation at 2-week (P = 0.029) and 4-weeks (P =0.0253) in the stroke group relative to sham, and at 1-week (P = 0.0084) and 4-week (P = 0.0261) in the stroke group compared to pre-stroke. Mixed Effects Model, Time $F_{(3.718, 42.39)} = 2.014$, P = 0.1141; Stroke Group $F_{(1, 13)} = 9.155$, P = 0.0097; Interaction $F_{(5, 57)} = 2.348$, P = 0.0524. In the distal imaging region, no significant main effects or interaction was found for the correlation coefficient for significantly correlated assembly-assembly pairs (**C**). Peri-infarct region Stroke N = 11, Sham N = 4. Distal region Stroke N = 13, Sham N = 4. *p < 0.05; **p < 0.01; ***p < 0.001